Environmental Science: Atmospheres

ROYAL SOCIETY OF CHEMISTRY

PAPER

View Article Online
View Journal | View Issue

Cite this: *Environ. Sci.: Atmos.*, 2022, **2**, 315

Aerosol optical properties and brown carbon in Mexico City†

Armando Retama, *[a] Mariana Ramos-Cerón,[b] Olivia Rivera-Hernández,[b] George Allen [c] and Erik Velasco [d]

Brown carbon (BrC) is a component of particulate matter which has significant impacts on climate forcing and air quality. To elucidate the current state and sources of BrC in Mexico City, the largest megacity in North America, the aerosols' ability to scatter and absorb light was evaluated over two years in concert with detailed chemical speciation of their components during a period of six months. These measurements made it possible to evaluate the seasonal and diurnal variations of the chemical composition, optical properties, and origin of BrC. It was found that 67% of the light extinction at 870 nm is due to scattering. Organic aerosols dominate the submicron mass loading (62%), as well as the light scattering (>50%). Nitrate and sulfate compounds are also important contributors to light scattering. Among the organic fraction, fresh particles strongly associated with traffic emissions dominate the light absorption at ultraviolet (UV) wavelengths on days not affected by biomass burning plumes. Regional wildfires are ubiquitous in the central region of Mexico during the dry-warm season (March–May) and can drastically increase the light scattering and absorption attributed to the organic fraction. During wildfire episodes, the organic fraction can contribute up to 80% and 50% to light scattering and absorption, respectively. Aged organic aerosols have a negligible contribution to light absorption at UV wavelengths, but secondary organic aerosols of recent formation contribute on average 24% in days not affected by wildfire plumes. Brown carbon and black carbon (BC) contributed 22% and 78% to the total light absorption in México City, respectively. Brown carbon increases on average 28% the light absorption over that attributed to BC. This increase can be up to 32% during the dry-warm season. In summary, vehicular traffic is the main contributor to BrC light absorption on a daily basis, while biomass burning becomes the major contributor during wildfire episodes.

Received 14th January 2022
Accepted 4th April 2022

DOI: 10.1039/d2ea00006g

rsc.li/esatmospheres

Environmental significance

Changes in urban emission profiles and atmospheric processes derived from new environmental regulations, growing urbanization and a changing climate modify the way aerosols interact with solar light. Therefore, it is necessary to evaluate the optical properties of aerosols along with their chemical composition, origin, seasonal variability, and diurnal photochemistry to mitigate their impact on air quality and radiative forcing. This is particularly true in large cities, such as Mexico City, where policies have failed to reduce the burden of organic and inorganic particles that modulate the extinction of light. Based on the results of this study, it is essential that programs to improve the urban atmosphere take into account the chemical and optical properties of aerosols.

1. Introduction

Atmospheric aerosols interact with sunlight and affect air quality and climate. They absorb and scatter light according to the optical properties resulting from their mass loading, size distribution, age, chemical composition, mixing state and hygroscopicity.[1] Therefore, the aerosols' ability to scatter and absorb light must be evaluated in conjunction with their chemical composition to determine their origin, and thus be able to design effective policies to mitigate their impact on air quality and climate forcing.[2,3] For example, in urban atmospheres organic aerosols and inorganic aerosols like sulfates (SO_4^{2-}), nitrates (NO_3^-) and ammonium (NH_4^+) dominate the scattering of light,[4] while carbonaceous aerosols, including black carbon (BC) and some organic aerosols (OA), dominate light absorption.[5]

Black carbon is an operational term commonly used to represent soot-like particulates produced by combustion of fossil fuel and biomass that strongly absorb light across the ultraviolet (UV) and visible spectral regions.[6] However, the

[a]*Independent Researcher, Mexico City, 11800, Mexico. E-mail: armando.retama@gmail.com*
[b]*Secretaría del Medio Ambiente de la Ciudad de México, Mexico City, 06068, Mexico*
[c]*Northeast States for Coordinated Air Use Management, Boston MA 02111, USA*
[d]*Independent Research Scientist, 118719, Singapore*

† Electronic supplementary information (ESI) available. See https://doi.org/10.1039/d2ea00006g

carbonaceous fraction includes also organic species with a nonuniform absorption over the spectral range (*i.e.*, increasing absorption toward the UV region), which gives them a brownish appearance instead of black, the reason they are named brown carbon (BrC).[7] The BrC composition is complex and depends on the aerosols' origin and atmospheric processes. Natural and anthropogenic humic-like substances (HULIS) and tarry material from combustion aerosols are well known sources of BrC.[5,8,9] Brown carbon can be also found as part of secondary OA (SOA),[10] while chemical aging can enhance the formation of chromophores and produce aerosol bleaching.[3]

The abundance of BrC and its complexity makes it necessary to evaluate *in situ* the aerosol optical properties to not overlook the climate and visibility effects of light-absorbing carbon, as well as to assess the impacts on photochemistry (*i.e.*, production of secondary pollutants) triggered by a decreased UV irradiance.[3] In urban environments, changes in the radiative balance resulting from aerosol pollution may be strong enough to alter the local micrometeorology, increase the urban heat island effect and enhance the accumulation of pollutants, in addition to affect the diurnal photochemistry.[11–13]

The impact of BrC on the optical properties of aerosols in urban atmospheres has been widely documented in recent years.[14–18] However, the light absorption and scattering response to changes in emission profiles and atmospheric processes that control the formation of secondary aerosols, as a result of growing urbanization, new environmental regulations, and a changing climate is still highly uncertain. An improved understanding of the origin and optical properties of BrC based on reliable measurements over periods long-enough to capture annual and seasonal variabilities is critically important to design effective emission control policies to improve air quality and mitigate climate change. For example, an accurate characterization of the BrC contribution to light absorption across different temporal scales is needed to interpret the aerosol optical depth (AOD) retrieved from remote sensing data that is widely used in climate model predictions and air quality assessments.[3,19]

In such context, this study investigates the diurnal and seasonal variations of the optical properties and chemical composition of the atmospheric aerosols in Mexico City, the largest city in North America, to determine the current state of BrC, and elucidate its origin and contribution to light absorption and scattering all year round.

The optical properties of the aerosols in Mexico City were assessed through studies of short duration (*i.e.*, weeks) in the past. The *Investigación sobre Materia Particulada y Deterioro Atmosférico* – Aerosol and Visibility Evaluation Research (IMADA-AVER) campaign in February–March 1997 provided insights into particulate composition and properties.[20–22] The intensive air quality field campaign Mexico City Metropolitan Area – 2003 (MCMA-2003) and the Megacity Initiative: Local and Global Research Observation in 2006 (MILAGRO) provided valuable information on the optical properties and chemical composition of the aerosols during the spring season under dry and warm weather conditions.[23–27] The optical properties were associated with combustion of fossil fuels within the city and regional biomass burning, as well as with the photochemical formation of secondary aerosols.[28–30] The ability of the aerosols to scatter and absorb light was linked to both warming of the atmospheric boundary layer[29,31] and changes in the photochemical production of secondary species.[32,33] Recent studies have determined the optical properties during longer periods using ground-based instrumentation,[34,35] and remote-sensing data,[36,37] but they have not simultaneously evaluated the chemical composition of the aerosols.

The information presented in this article should help to design future strategies to improve air quality and mitigate climate change at local and regional scales, and act as a reference for other large cities of developing nations facing similar air quality problems. In terms of local climate, little is known about the aerosols' role in the warming of the city, despite a consistent upward trend in ambient temperature.[38] Similarly, poor visibility is a persistent problem that has not received enough attention. Regarding air quality, Mexico City has not been able to reduce ambient concentrations of particulate matter (PM) smaller than 2.5 μm in size ($PM_{2.5}$) during nearly two decades despite important reductions in other key pollutants, such as sulfur dioxide (SO_2), carbon monoxide (CO) and nitrogen oxides (NO_X), as well as in a number of volatile organic compounds (VOCs) associated with anthropogenic emissions.[39] Secondary organic aerosols dominate the $PM_{2.5}$ burden and are rapidly produced from the atmospheric oxidation of VOCs through the formation of low-volatility oxidation products,[40] thus any change in the VOC budget may affect the formation of SOA, and in turn the aerosol optical properties.

2. Methods

The aerosol optical properties were monitored using a Photoacoustic Extinctiometer (PAX) (Droplet Measurement Technologies, Boulder, CO, USA) and a Dual-spot Aethalometer® AE33 (Magee Scientific, Berkeley, CA, USA) for 25 months (June 2017 to June 2019). The former instrument was used for simultaneous measurements of aerosol scattering and absorption coefficients, and the latter for measurements of aerosol light attenuation at different wavelengths. Additional instrumentation used to investigate the impact of the aerosols' mass concentration and chemical composition on the variability of the optical properties included a Tapered Element Oscillating Microbalance instrument (TEOM Model 1400AB, Rupprecht & Patashnik Co., Inc., Albany, NY) and an Aerosol Chemical Speciation Monitor (ACSM, Aerodyne Research Inc., Billerica, MA, USA). PAX and AE33 collected data every minute, TEOM provided hourly averages of PM mass concentration, while the ACSM collected data every ~30 minutes.

The ambient concentrations of CO and NO_X were measured as tracers of specific emission sources (*e.g.*, vehicular traffic), while concentrations of ozone (O_3) were measured as an indicator of photochemical activity. These gaseous pollutants were measured using continuous monitors based on the United States Environmental Protection Agency (US-EPA) reference or equivalent methods. Carbon monoxide was measured by a non-dispersive infrared analyzer with gas filter correlation (model

300E, Teledyne API, San Diego, CA), NO_X by a chemiluminescence analyzer (model 200E, Teledyne API, San Diego, CA), and O_3 by a UV absorption analyzer (model 400E, Teledyne API, San Diego, CA). These instruments collected data every minute. The response of each analyzer was verified once per week, while calibrations were performed every third month using standard gases.

The Environmental Analysis Laboratory of Mexico City's Secretariat for the Environment, located 9 km northwest of the city center (19°29′01.44″N, 99°08′50.21″W, 2243 m above sea level), was used as monitoring site. A mix of low-rise households, commercial establishments and light industries surround the site. Plumes associated with north winds from a major industrial district and densely populated neighborhoods at the city's outskirts are frequent. The site is affected by two roads with heavy traffic located both at a distance of 500 m. A map showing the location of the monitoring site is included in the ESI (Fig. S1†).

This site has been previously used to investigate different aspects of Mexico City's air pollution.[34,41,42] The supersite used to characterize the urban plume during the IMADA-AVER and MILAGRO field campaigns was located about 700 m to the north. This area of the city has demonstrated to provide representative information on the pollutants mix, especially of fresh emissions of precursor species.

Detailed descriptions of the instruments used in this study, as well as the data analysis performed to elucidate the optical properties of the aerosols are provided below. The section starts with a brief description of Mexico City's climate and its influence on the aerosols' burden and properties, then describes the instruments' fundamentals and operation, and at the end explains the approaches followed to determine the absorption Ångström exponent, the light absorption associated with BrC and individual groups of organic aerosols, and the influence of aerosols chemical composition on light scattering.

2.1 Mexico City's climate

Mexico City has a subtropical highland climate defined by three distinctive climatological seasons: a dry-warm season from February to May followed by a rainy season until October, and a dry-cool season from November to February. The dry-warm season presents high pressure systems with clear skies, high solar radiation, and weak wind most of the days, conditions that enhance the production and buildup of photochemical pollutants such as O_3 and secondary aerosols. Regional wildfires are common during this season, especially in croplands since open field burning is a common practice to remove the stubble after harvest in Mexico.[43] The rainy season presents lower levels of PM pollution, despite intense photochemical activity before the almost daily afternoon precipitations. The dry-cool season is characterized by frequent and stronger surface thermal inversions, which enhance the accumulation of primary emitted PM and gaseous pollutants. Although less frequent, plumes from cropland fires in the region can also reach the city during this season. A detailed back trajectory analysis of plumes originated from regional fires, and time series of the main meteorological variables measured during this study are included in the ESI (Text S1 and Fig. S2,† respectively).

2.2 Instrumentation

2.2.1 Photoacoustic Extinctiometer. The PAX measures directly the light-absorption and -scattering coefficients, b_{abs} and b_{scat}, at 870 nm using simultaneously a photoacoustic resonator and a nephelometer. A complete description of the instrument is provided by the manufacturer,[44] while Retama *et al.*[34] describe its operation and performance for Mexico City's atmospheric conditions. Briefly, for the absorption measurements a laser beam directed through the sample's stream is modulated at ~1500 Hz. Light-absorbing particles heat up quickly and transfer heat to the surrounding air producing sound waves that are detected by a microphone located on the top of the absorption cell. From the amplitude of the sound wave, b_{abs} is then calculated. In contrast to filter-based absorption instruments, the PAX directly measures absorption on the sample while it is suspended in the air, avoiding filter artifacts. To measure b_{scat} the PAX uses a wide-angle (6–174°) integrating reciprocal nephelometer that responds to all particle types. The simultaneous measurement of both coefficients allows to derive the extinction coefficient ($b_{ext} = b_{scat} + b_{abs}$) and single scattering albedo (SSA = b_{scat}/b_{ext}). The absorption coefficient is also used to calculate the BC mass concentration assuming a mass absorption cross-section (MAC) of 4.74 $m^2\ g^{-1}$. The major uncertainty associated with the PAX for measuring BC comes from the MAC selection, as it does for any other instrument based on light-absorption, thus the term equivalent BC (eBC) is a more appropriate term as pointed out by Petzold *et al.*[6] The instrument was factory calibrated at the beginning of the study, while the flow, clean air response and operating parameters were continuously verified.

The sample inlet was placed at 1.8 m above roof level (5.2 m above ground level). The PAX and other particle analyzers were kept in an air-conditioned room. A sampling system was built using a 16.67 L min^{-1} PM_{10} inlet (BGI Inc., Waltham, MA) coupled to a PM_1 sharp cut cyclone (SCC 2.229, BGI Inc., Waltham, MA). A diffusion Nafion dryer (Perma Pure LLC, Lakewood, NJ) was used to minimize relative humidity effects. An external pump provided additional flow for the inlet and the diffusion dryer. Relative humidity was maintained under 35%. The sampling flow rate was verified every week to maintain the PAX operating at a flow rate of 1 L min^{-1}. An isokinetic flow splitter was used to provide sampling flow to both PAX and Aethalometer.

2.2.2 Dual-spot Aethalometer. A dual-spot Aethalometer was used for aerosol light attenuation measurements at seven wavelengths (λ = 370, 470, 520, 590, 660, 880 and 950 nm) under a sampling flow rate of 2 L min^{-1} and a 1 min temporal resolution. A detailed description of the instrument is provided by Drinovec *et al.*[45] Briefly, the Aethalometer measures the attenuation coefficient (b_{ATN}) of a light beam transmitted through a filter tape loaded with aerosol samples. To compensate the aerosol loading effect, the dual-spot method measures simultaneously the light attenuation on two sample spots with

different loadings. This approach eliminates the nonlinear loading effect related to filter aerosol saturation. However, the multiple scattering of light within the filter material might still affect the optical attenuation. To account for this artifact a correction parameter C is used to obtain a representative b_{abs} value under the assumption that the wavelength dependence of C is negligible.[46,47]

$$b_{abs}(\lambda) = b_{ATN}/C \quad (1)$$

Based on a series of field and laboratory observations, the manufacturer suggests a C value of 1.57 for polytetrafluoroethylene (PTFE)-glass fiber filters (TX40-Emfab, tape model 8050) and 1.37 for polyethyleneterephthalate (PET)-glass fiber filters (tape model 8060). However, to account for scattering artifacts related to the properties of local aerosols, it is recommended to adjust *in situ* this correction parameter.[48,49] Thus, a site-specific multiple-scattering correction factor (C_{ref}) was obtained for each filter tape used during the study taking as reference the b_{abs} measured by PAX, as it is not affected by filter interferences.

The PAX was considered as reference instrument for determining b_{abs}, since it is much less affected by scattering artifacts, such as those derived from the amount of particles deposited on the filter and the filter material, which together induce a positive bias in light attenuation in the case of the AE33 Aethalometer. Kalbermatter *et al.*[50] compared the performance of different instruments for measuring aerosol absorption with laboratory-generated soot particles, and found uncertainties close to zero for the case of PAX and 20–50% for the case of the AE33 Aethalometer. For the particular case of Mexico City, in a previous study we determined PAX uncertainties <3 Mm^{-1}, which are lower than the absorption coefficients typically observed at ambient level (16–42 Mm^{-1}, see Table 1). This uncertainty is mainly related to the accuracy of the calibration and the losses in the inlet system, and triggers errors no larger than 20%.[34]

C_{ref} was calculated using b_{ATN} readings at 880 nm depicting attenuations <10% from readings during the previous filter step (*i.e.*, $\Delta b_{ATN,880}$ < 10%, $b_{ATN\Delta 10,880}$), and PAX b_{abs} readings at 870 nm approximated to 880 nm (PAX $b_{abs,880}$).

$$C_{ref} = b_{ATN\Delta 10,880}/\text{PAX } b_{abs,880} \quad (2)$$

The application of a locally derived C_{ref} improved the Aethalometer's performance. A strong correlation (r^2 = 0.94–0.99) and slopes close to one between both instruments were achieved in this manner. The correction factor recommended by the Aethalometer's manufacturer overestimated by a factor of two the b_{abs} values obtained from PAX. Our results suggest that a value of 3.5 is acceptable for the multiple-scattering correction in Mexico City using any type of filter (Table S1†). Fig. S3† compares the b_{abs} values returned by both instruments using C and C_{ref} to compensate the Aethalometer readings.

Recent studies have reported shortcomings for measuring b_{abs} at short wavelengths when using the filter tape 8050,[51] the manufacturer recommends using a flow rate of 2 L min^{-1} to reduce such errors.[52] Our Aethalometer was initially equipped with such tape for a period of one year (June 2016–May 2017), then it was replaced by filter tape model 8060. As already mentioned, similar C_{ref} were obtained for both filter tape models, but the former yielded a slightly higher variability in the readings of b_{abs} at 880 nm. Compared to the readings obtained from PAX, the former and latter tape models yielded root-mean-square deviations of 3.4 and 1.8, respectively.

2.2.3 PM_1 mass concentration and chemical composition. A TEOM instrument coupled with an 8500 Filter Dynamics Measurement System (FDMS) measured continuously mass concentrations of PM smaller than 1 μm (PM_1). Samples were taken from a 7.2 m height inlet equipped with a PM_1 sharp-cut cyclone (SCC 2.229, BGI Inc., Waltham, MA) at a flow rate of 16.67 L min^{-1}.

An ACSM was used for a period of six months (December 2018 to June 2019) to measure mass concentrations of speciated non-refractory submicron particles (NR-PM_1), including SO_4^{2-}, NO_3^-, NH_4^+, chloride (Cl^-) and organics. Using an array of aerodynamic lenses, the ACSM focuses individual particles into a beam, non-refractory components are vaporized at ~600 °C, ionized by a 70 eV electron impactor, and analyzed with a quadrupole mass spectrometer.[53] Air was sampled at 5 L min^{-1} through a $PM_{2.5}$ Teflon coated aluminum inlet (URG Corporation, Chapel Hill, NC) and dried in a multi-tube Nafion dryer (model PD-50T-12-MSS, Perma Pure LLC, Lakewood, NJ) before entering the instrument. The ACSM response factor was calibrated for NO_3^- standard, and the relative ionization efficiencies for NH_4^+ and SO_4^{2-} were verified before the measurement period. A collection efficiency factor of 0.5 was used to account for the incomplete detection of particles.[42]

The aerosol mass spectra were deconvolved and analyzed using the Positive Matrix Factorization (PMF) version 4.2 [54] and the PMF Evaluation Tool (PET) version 2.08D.[55] After inspecting the spectral profiles and correlations with representative source emission tracers, four factors of non-refractory organic aerosols were determined: more oxidized oxygenated organic aerosols (MO-OOA), less oxidized oxygenated organic aerosol (LO-OOA), biomass burning organic aerosols (BBOA) and hydrocarbon-like organic aerosols (HOA). The deconvolved mass-spectra are presented in Fig. S4.† The MO-OOA and LO-OOA groups represent SOA; the former group is a surrogate of highly aged aerosols with an important regional character, while the latter is associated with less photochemical aged aerosols.[56] HOA portrays primary aerosols, thus it is correlated with CO, NO_X, and fresh traffic emissions in general. The signals associated with anhydrous sugars present in biomass smoke were used to determine the BBOA group as suggested by Alfarra *et al.*[57] Fragments of anhydrous sugars, such as levoglucosan (m/z 60 and m/z 73) can also be found in emissions of coal combustion, and cooking.[58,59] Coal is not used as fuel in Mexico City, but cooking does have a contribution that should be addressed in future studies. Similarly, these molecules are highly oxidized and can add to the aged aerosols load.[60] However, in our case their contribution to MO-OOA was null, as shown in its resolved mass spectra (see Fig. S4†).

Table 1 Statistical metrics of the aerosol optical properties measured by the Aethalometer AE33 and PAX instruments, and air pollutants and meteorological variables measured during the entire study (June 2017 to June 2019). The number of valid hours (N) along with the geometric and arithmetic means and standard deviations (μ_G [σ_G] and $\mu \pm \sigma$, respectively), median, 25th to 75th percentiles, and maximum values are presented for each parameter

Parameter	N	μ_G [σ_G]	$\mu \pm \sigma$	Median	25th to 75th percentiles	Max
Aethalometer AE33						
$b_{abs,370}$ (Mm^{-1})	16 958	25.5 [2.1]	33.1 ± 27.0	25.2	15.6–41.6	329.3
$b_{abs,470}$ (Mm^{-1})	16 958	19.0 [2.1]	24.8 ± 20.3	18.6	11.5–31.1	241.9
$b_{abs,520}$ (Mm^{-1})	16 958	16.4 [2.1]	21.4 ± 17.6	16.1	9.9–27.0	202.2
$b_{abs,590}$ (Mm^{-1})	16 958	14.3 [2.1]	18.7 ± 15.5	14.0	8.6–23.6	171.8
$b_{abs,660}$ (Mm^{-1})	16 958	12.3 [2.1]	16.1 ± 13.2	12.0	7.4–20.3	145.8
$b_{abs,880}$ (Mm^{-1})	16 958	9.0 [2.1]	11.8 ± 9.8	8.7	5.4–14.9	100.3
$b_{abs,950}$ (Mm^{-1})	16 958	8.4 [2.1]	11.0 ± 9.2	8.1	5.0–13.9	93.7
AAE	16 958	1.18 [1.12]	1.19 ± 0.14	1.16	1.09–1.25	2.56
Photoacoustic extinctiometer						
eBC ($\mu g\ m^{-3}$)	15 257	2.0 [2.0]	2.6 ± 2.0	1.9	1.3–3.2	24.2
$b_{abs,870}$ (Mm^{-1})	15 257	9.5 [2.0]	12.1 ± 9.5	9.2	5.9–15.2	114.8
$b_{scat,870}$ (Mm^{-1})	14 921	20.6 [2.0]	26.2 ± 18.9	21.8	12.9–34.5	242.5
$b_{ext,870}$ (Mm^{-1})	14 921	31.6 [1.9]	38.4 ± 24.7	33.0	20.4–50.4	304.1
SSA	14 921	0.7 [1.2]	0.7 ± 0.1	0.7	0.6–0.8	0.9
Air pollutants and meteorology						
PM_1 ($\mu g\ m^{-3}$)	16 633	17.2 [2.1]	21.4 ± 13.5	19.0	11.5–28.6	161.9
CO (ppb)	13 724	331 [2]	459 ± 401	330	188–590	3230
NO_X (ppb)	15 376	41 [2]	57 ± 52	40	22–74	434
O_3 (ppb)	14 928	15 [4]	30 ± 30	19	5–47	157
Temperature (°C)	17 473	16.3 [1.4]	17.1 ± 4.9	16.5	13.9–20.3	32.6
Relative humidity (%)	17 352	52 [1.6]	57 ± 23	57	38–77	100
Wind speed ($m\ s^{-1}$)	17 622	1.6 [1.8]	1.8 ± 1.0	1.7	1.1–2.5	7.0

2.3 Analysis methods

2.3.1 Absorption Ångström exponent. The absorption Ångström exponent (AAE) describes the wavelength dependence of b_{abs} depicted by a power law function as a dimensionless value derived from measurements of the aerosols thickness at different wavelengths.[61] This exponent responds to the size, shape, and chemical composition of the particles, thus it can be used as a tool to identify the aerosols' origin. For example, aerosols produced by combustion of fossil fuels yield AAE values of 0.8–1.1,[62] while those resulting from biomass burning of 0.9–3.5.[63,64] Due to a dominant presence of aerosols from vehicular traffic, the urban mix of aerosols usually shows AAE values around one.[62,65]

The slope obtained from the linear regression between the log-transformed b_{abs} and wavelength spectra was used to obtain the hourly AAE values. Fig. 1 shows the power law wavelength dependence of b_{abs} for the three climatological seasons of Mexico City.

2.3.2 Brown carbon light absorption. The presence and abundance of BrC can be assessed through the light absorption in the UV-visible region following the AAE segregation method using b_{abs} data at short and long wavelengths.[66,67] This method derives the BrC absorption ($b_{abs,BrC}$) at a specific short wavelength (*e.g.*, 370 nm) as the difference between the total aerosol absorption ($b_{abs,370}$) and the absorptions related to BC at 370 nm ($b_{abs,BC,370}$). We considered the absorption of non-carbonaceous aerosols (*e.g.*, mineral dust, biological materials) as negligible due to its limited contribution to the submicron fraction.[68]

$$b_{abs,BrC,370} = b_{abs,370} - b_{abs,BC,370} \quad (3)$$

The total $b_{abs,370}$ was directly measured by the Aethalometer, while $b_{abs,BC,370}$ was extrapolated from the $b_{abs,BC}$

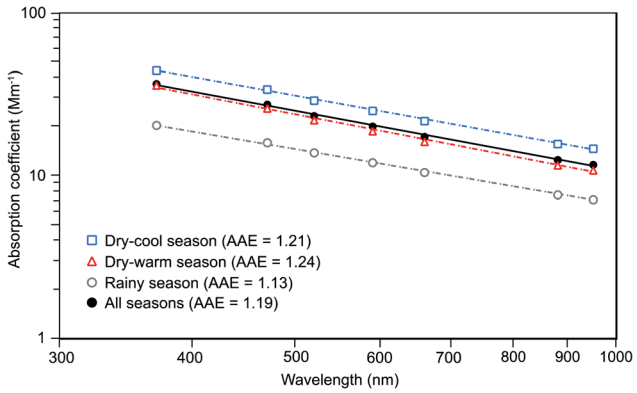

Fig. 1 Power law distributions of absorption coefficients for the 370–950 nm wavelength range as measured by the Aethalometer AE33 for each climatological season of Mexico City and during the two-year study. The AAE values are the arithmetic means obtained from the linear regressions between the log-transformed hourly b_{abs} records and wavelength spectra, considering the full study period, and individual climatological seasons.

measurements at 950 nm using the AAE value attributed to BC (AAE_{BC}). The UV absorption was assumed negligible at this long wavelength.

$$b_{abs,BC,370} = b_{abs,BC,950} \times (950/370)^{AAE_{BC}} \quad (4)$$

The choice of AAE_{BC} is critical for the correct attribution of $b_{abs,BC,370}$.[67,69] An AAE_{BC} value of 1.0 is often adopted, despite studies have found it might vary according to the BC core, particle size, morphology, mixing state and coating thickness of the particles.[70,71] The impact of these variables can be approximated by the Mie theory using the aerosol size distribution data.[72] In the absence of such data, we followed the "two-wavelength approach" proposed by Al Fischer and Smith[73] to calculate AAE_{BC} from b_{abs} measurements at 880 and 950 nm, at which BrC is expected to have a null or very minor contribution:

$$AAE_{BC} = \frac{\ln\left(\frac{b_{abs,880}}{b_{abs,950}}\right)}{\ln\left(\frac{880}{950}\right)} \quad (5)$$

A median AAE_{BC} hourly value of 0.88 was obtained along the 2 year study with an interquartile range of 0.84–0.95, after discarding 8 of 16 958 readings in which $b_{abs,880} > b_{abs,950}$, and the condition of AAE > 0 was not met.[67]

2.3.3 Mass scattering efficiency and single scattering albedo. The mass scattering efficiency (MSE) is a measure of the aerosol light scattering per mass of aerosol and has an important role in visibility degradation and radiative forcing. It is defined as the ratio between b_{scat} and mass concentration. In this study, it was obtained from the slope between $b_{scat,870}$ and PM_1 measured by PAX and TEOM, respectively, and represents the average efficiency observed during the entire study under different climatological conditions and particle loads.

The SSA is the fraction of light scattering over the sum of light scattering and absorption (extinction). It is a critical parameter to determine the impact of aerosol light-absorbtion on the radiative balance. The SSA at 870 nm was calculated from the scattering and extinction coefficients measured by PAX (see diurnal variability in Fig. 2i and time series of daily means in Fig. S6†). The SSA values range from 0 to 1, a value of 1 represents a purely scattering particle (or population), and 0 represents a purely absorbing one.

2.3.4 Mass absorption contribution by group of organic aerosols. The mass-weighted absorption efficiency (MAE) is used as a proxy to relate the particle mass concentration in air and the absorption coefficient. The individual MAE for each

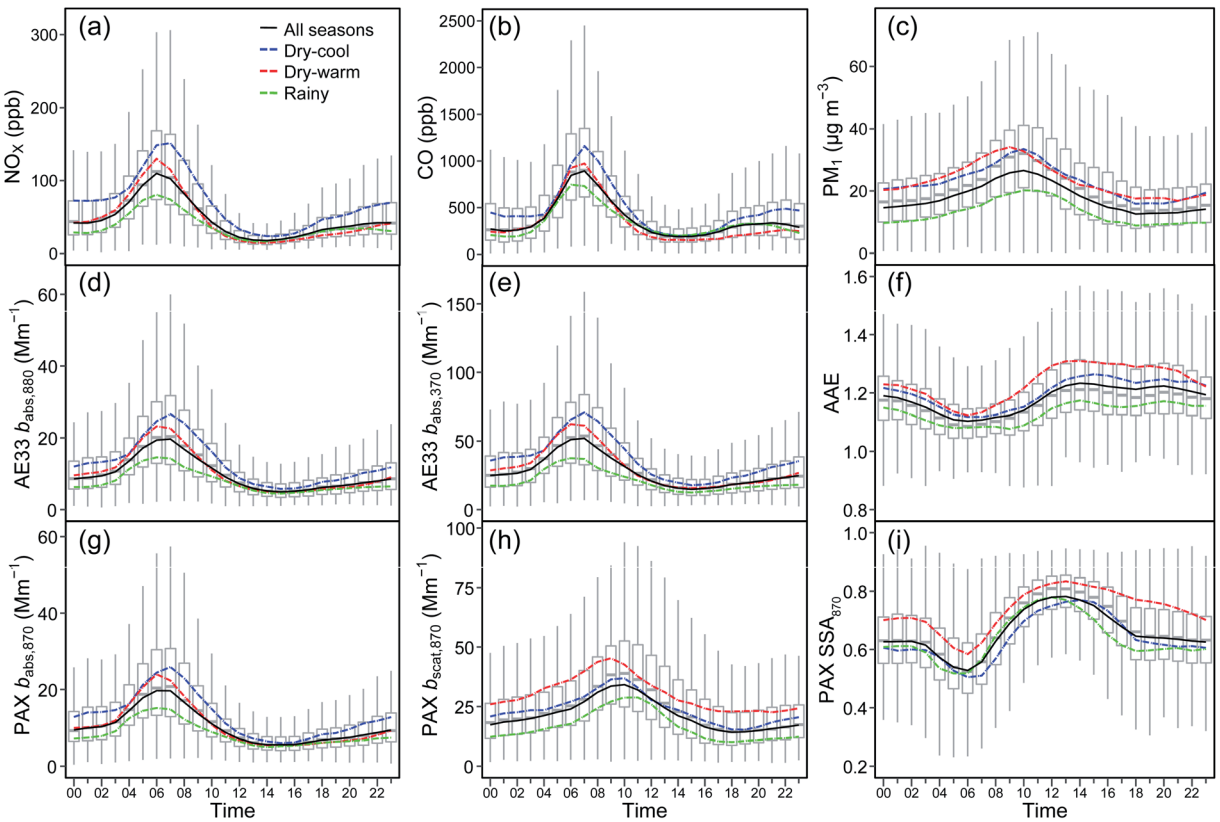

Fig. 2 Diurnal cycle of (a) NO_X, (b) CO, (c) PM_1, (d–f) selected aerosol optical properties obtained from the Aethalometer AE33 and (g–i) PAX measurements. The box plots show the hourly variability considering the two-year dataset, in each box the middle line, top and bottom are median value, upper and lower quartile (75th and 25th percentiles), respectively, and whiskers extend 1.5 times the interquartile range. The black solid line shows the hourly geometric means for the full dataset. The blue, red, and green dashed lines indicate the hourly geometric means for each climatological season.

group of organic aerosols as defined by PMF can be obtained from the correlation factors that determine the total aerosol light mass absorption as expressed by eqn (6). Considering no cross-interactions between groups, the correlation factors can be solved by a multiple linear least-square regression analysis.[17] The product of the mean mass concentration (μg m^{-3}) of each individual group and corresponding MAE (m^2 g^{-1}) yields its contribution to the net mass absorption by OA (Mm^{-1}).

$$b_{abs,BrC,370} = MAE_{HOA}[HOA] + MAE_{BBOA}[BBOA] + MAE_{LO\text{-}OOA}[LO\text{-}OOA] + MAE_{MO\text{-}OOA}[MO\text{-}OOA] \quad (6)$$

2.3.5 Light scattering reconstruction. Particles between 0.1 and 1 μm yield the highest scattering efficiency in the visible range,[74] thus a strong correlation between PM_1 and the particle scattering coefficient ($b_{scat,870}$) can be expected. Nitrate, SO_4^{2-}, NH_4^+ and the organic fraction in PM_1 contribute most to light scattering.[75] These chemical species interact distinctly with light depending on the particle's size, composition, water content and mixing state. In the air, ions form neutral species, then assuming that the particles are internally mixed, the correlation between light scattering and the ion-pairing species can be evaluated including the contribution of inorganic and organic species through the revised version of the equation used by the Interagency Monitoring of Protected Visual Environments (IMPROVE) program of the US-EPA to determine light extinction[76] in conjunction with a modified ion pairing scheme.

The IMPROVE equation reconstructs the light extinction based on aerosol mass and size using a multiple linear regression method that considers the degree to which aerosol light scattering is related to the mass concentration of each component combined with water uptake. However, in our case the sampling stream was dried before being analyzed, thus the humidity influence on the particles' growth was neglected. The original equation uses a threshold of 20 μg m^{-3} to apportion the mass in large and small particles,[76] but it was found it allocates too much mass into the small size mode, which has a lower dry mass scattering efficiency leading to a persistent underestimation of light scattering. To avoid such potential bias, we replaced the original threshold value by five times the median mass of each component as suggested by Prenni *et al.*[4] The revised IMPROVE equation also includes contributions of soil and sea-salt, which we neglected in this study. The NR-organic fraction measured by the ACSM was used as surrogate of organic mass (OM). The use of a 1 μm cut-size inlet excluded soil-related particles, and the city is far enough from the coast. The equation simplifies as follows for our case, considering the aerosol concentrations in μg m^{-3} and the light scattering in Mm^{-1}.

$$b_{scat,870} \approx \left(2.2 \times \left[(NH_4)_2SO_4\right]_{small} + 4.8 \times \left[(NH_4)_2SO_4\right]_{large}\right) + \left(2.4 \times [NH_4NO_3]_{small} + 5.1 \times [NH_4NO_3]_{large}\right) + \left(2.8 \times [OM]_{small} + 6.1 \times [OM]_{large}\right) \quad (7)$$

Major ions such as ammonium sulfate, $(NH_4)_2SO_4$, and ammonium nitrate, NH_4NO_3 were assumed to be fully neutralized. The concentrations of inorganic components in eqn (7) were approximated using an ion pairing scheme, in which SO_4^{2-} is neutralized by NH_4^+, and the excess of NH_4^+ is used to neutralize NO_3^-.[77,78] This scheme was modified to include the neutralization of NH_4^+ by Cl^-, since its levels in Mexico City are not negligible, particularly during the dry-cool season.[79,80] The ion-paring scheme applied in this study is summarized as:

$$\begin{aligned} n_{H_2SO_4} &= \max\left(0,\ n_{SO_4^{2-}} - n_{NH_4^+}\right), \\ n_{NH_4HSO_4} &= \min\left(2n_{SO_4^{2-}} - n_{NH_4^+},\ n_{NH_4^+}\right), \\ n_{(NH_4)_2SO_4} &= \min\left(\max\left(n_{NH_4^+} - n_{SO_4^{2-}},\ 0\right),\ n_{SO_4^{2-}}\right), \\ n_{NH_4NO_3} &= \min\left(\max\left(n_{NH_4^+} - 2n_{SO_4^{2-}},\ 0\right),\ n_{NO_3^+}\right), \\ n_{NH_4Cl} &= \min\left(\max\left(n_{NH_4^+} - 2n_{SO_4^{2-}} - n_{NO_3^+},\ 0\right),\ n_{Cl^-}\right) \end{aligned} \quad (8)$$

where n is the number of moles. This scheme must be taken only as an approximation to the formation of inorganic salts, the assumption of internal mixing does not adequately describe the thermodynamic equilibriums, nor the competition between SO_4^{2-}, NO_3^- and Cl^- for NH_4^+, while the role of organic nitrates is neglected.[77,78,81]

3. Results and discussion

An initial inspection of the b_{abs} and b_{scat} measurements showed a positive highly skewed distribution (*i.e.*, lognormal distribution). We applied the Kolmogorov–Smirnov statistical test to verify the lack of normality in both datasets ($p < 0.05$). The use of geometric averages and standard deviations (μ_G, σ_G) was chosen over the use of arithmetic averages and standard deviations (μ, σ) to evaluate the variability of the optical coefficients. Unless otherwise noted in the text, the discussion presented here is based on geometric parameters; note that σ_G is a multiplicative factor, and thus dimensionless, it accounts for the range σ_G $[x]^{\pm 1}$ (*i.e.*, μ_G/σ_G to $\mu_G \times \sigma_G$). For comparison purposes with other studies, or when the data follow a normal distribution, arithmetic averages and standard deviations are used. Table 1 shows both sets of statistical metrics for the aerosol optical properties and air quality and meteorological variables measured throughout the study. The statistical metrics for each climatological season and time series of daily means are available in the ESI (Table S2 and Fig. S2†). The *R* statistical package was used for data handling and statistical tests, and the SAS statistical package for multiple linear regression analyses. All data are reported in UTC-6 time format (*i.e.*, local standard time), and no daylight-saving time was applied.

3.1 Aerosol absorption coefficients

The b_{abs} obtained from both instruments, PAX and Aethalometer AE33, showed diurnal patterns like those observed for NO_X and CO (Fig. 2). The strong correlations observed between b_{abs} and these traffic emission tracers (*e.g.*, for AE33 b_{abs} at 880 nm: $r^2 = 0.77$ for NO_X, and $r^2 = 0.69$ for CO) suggest that

exhaust particles regulate light absorption. Since these correlations are similar throughout the diurnal course, the magnitude of b_{abs} apparently relies on the airmass origin, and particles' dilution into an evolving convective boundary layer, as previously pointed out by Retama *et al.*[34] and Baumgardner *et al.*[28] Local biomass burning is not a contributing factor like in regions where the burning of wood and coal for domestic heating is necessary.[82,83] However, regional wildfires are important contributors during the dry-warm season.

The dry-cool season recorded the highest AE33 b_{abs} geometric means, 33.8 [2.1] (11.6 [2.1]) Mm^{-1} at 370 (880) nm. The second highest means were observed during the dry-warm season, 27.5 [2.0] (9.2 [2.0]) Mm^{-1}, while the lowest during the rainy season, 19.8 [1.9] (7.3 [2.0]) Mm^{-1}. Significant p-values ($p < 0.05$) for Mood's median test indicate that not all medians among seasons were equal. The high values during the dry-cool season responded to an enhanced accumulation of primary emitted particles in a generally shallower boundary layer characterized by increased atmospheric stability and frequent thermal inversions, which prevented the cleaning of the atmosphere by dilution and ventilation.[84] A stronger irradiance during the dry-warm season enhanced the release of heat from the urban surface along the night and early morning, which in turn favored the evolution of the boundary layer and pollutants' dilution. The low values during the rainy season were due to wind and turbulent conditions that increased atmospheric instability, thus preventing a significant accumulation of particles.

Previous studies in Mexico City reported similar diurnal patterns, but higher b_{abs} values. For example, Marley *et al.*[29] reported an arithmetic mean of 37 Mm^{-1} at 550 nm during the dry-warm season of 2006 at the nearby supersite equipped for the MILAGRO field campaign. This value exceeds the 19 and 22 Mm^{-1} obtained as means in this study at 590 and 520 nm, respectively. Similarly, Paredes-Miranda *et al.*[31] reported b_{abs} values ranging from 22 to 66 Mm^{-1} at 532 nm for a site at the southeast of the city in April 2003. More recently, Liñán-Abanto *et al.*[35] reported arithmetic means essentially equal to those observed in this study for each climatological season in the southwest of the city (see Table S2†). The lower light absorption is consistent with a reduction in emissions of BC as reported by the official emissions inventory within the political boundaries of the city during the last decade. In 2008, 1071 tons of BC were reported, while in 2018, 46% less.[85,86]

3.2 Aerosol scattering coefficient

A strong correlation between $b_{scat,870}$ and PM_1 was observed throughout the two-year study. The MSE yielded a value of 1.17 $m^2\ g^{-1}$ ($r^2 = 0.74$), experiencing some variations across the year. The dry-warm season reported the highest value (1.40 $m^2\ g^{-1}$, $r^2 = 0.77$), followed by the rainy season (1.21 $m^2\ g^{-1}$, $r^2 = 0.76$) and the dry-cool season (1.03 $m^2\ g^{-1}$, $r^2 = 0.71$). These MSE values were lower than those previously reported for a site at the southwest of the city for $PM_{2.5}$ of 1.86, 1.35, and 1.88 $m^2\ g^{-1}$ during the cold dry, warm dry and rainy seasons, respectively.[35] The larger cut-size of the particles and the fact that in such study[35] they were not dried prior to analysis explain the differences.

The light-scattering coefficient at 870 nm showed a consistent diurnal pattern all year round, with higher values in the morning and lower in the evening (Fig. 2h). Maximums were attained at 9–11 h, when the photochemical production of secondary aerosols jump starts and the ambient temperature is still not high enough to volatilize some aerosol's components; a similar pattern was observed by Paredes-Miranda *et al.*[31] During the dry-warm season the maximum values were recorded one and two hours earlier than during the dry-cool and rainy seasons, respectively. Values were also consistently higher during the dry-warm season, demonstrating the strong dependence of light scattering on the photochemical production of secondary aerosols, as well as on aerosol thermodynamics.[87,88] The lower b_{scat} values during the rainy season corresponded to frequent cloudiness, which limited the photochemical production of aerosols.

3.3 Aerosol single scattering albedo

The aerosol SSA showed an arithmetic mean of 0.67 ± 0.13 throughout the two years of study, and 0.74 ± 0.11, 0.65 ± 0.14, and 0.65 ± 0.12 during the dry-warm, rainy, and dry-cool seasons, respectively. The SSA values for the latter two seasons were similar to those reported by Liñán-Abanto *et al.*,[35] who found a constant arithmetic mean of 0.66 all year round. The SSA value reported in this study for the dry-warm season agrees with the value of 0.73 reported by Marley *et al.*[29] from data collected in March 2006. The higher SSA values during this season respond to the ubiquitous wildfires in the central region of Mexico[43] and an increased photochemical activity that enhances the formation of secondary aerosols,[31] both of which increase the burden of light-scattering capacity aerosols, as observed in the elevated concentrations of PM_1 and the SSA ratio from February to May. Wildfires also emit-light absorbing particles, but their rapid chemical evolution within the smoke plume favors the production of light-scattering particles.[89]

With respect to the diurnal variability, minimum SSA ratios (0.50–0.60) were observed during the morning rush hour, when light absorption was maximum and freshly emitted particles dominated the aerosol's burden, while maximum values were observed (0.75–0.85) in the early afternoon. The rapid increase during the morning and peaking around noon responded to the photochemical formation of secondary aerosols as explained by Paredes-Miranda *et al.*[31]

3.4 Absorption Ångström exponent

The hourly AAE values obtained from the linear regression between the log-transformed b_{abs} and wavelength spectra for each hour yielded an arithmetic mean of 1.19 ± 0.14 during the two-year study, while means of 1.21 ± 0.14, 1.24 ± 0.17, and 1.13 ± 0.10 were obtained for the dry-cool, dry warm, and rainy seasons, respectively (Fig. 1).

The AAE values observed in this study are like those reported for urban atmospheres highly impacted by vehicular

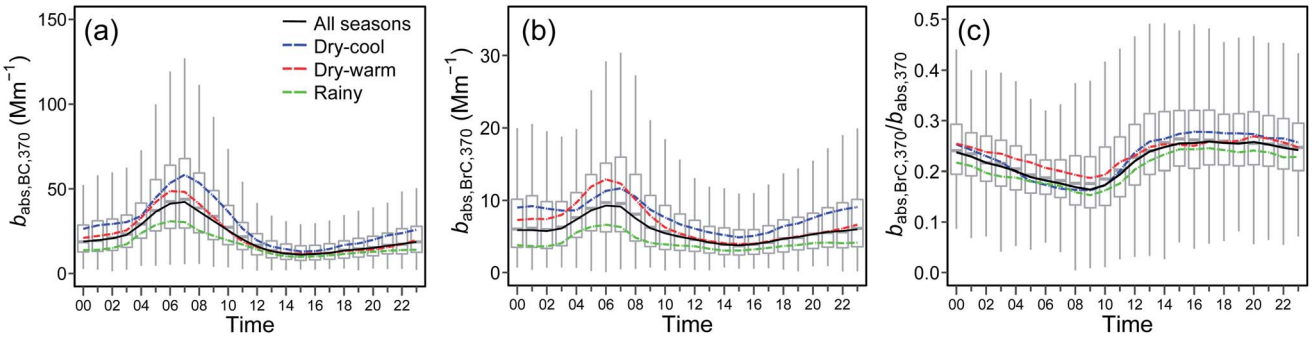

Fig. 3 Diurnal variability of the light absorption coefficients for (a) BC and (b) BrC, and (c) BrC contribution to the net b_{abs} at 370 nm. Box plots show the hourly variability considering the two-year dataset, in each box the middle line, top and bottom are median values, upper and lower quartiles (75th and 25th percentiles), respectively, and whiskers extend 1.5 times the interquartile range. The black solid lines show the hourly geometric means for the full dataset. The blue, red, and green dashed lines indicate the hourly geometric means for each climatological season.

traffic,[62,65,90,91] but lower than those impacted by woodsmoke and regional biomass burning.[92–94]

Previous studies in Mexico City based on similar instrumentation reported lower AAE values. For example, mean values of 1.05 (ranging from 0.76 to 1.50) and 0.94 (ranging from 0.63 to 1.40) were observed during the dry-warm seasons of 2003 and 2006, respectively.[30] The absence of filter-loading correction partially explain their lower AAE values. The two dry-warm seasons covered in this study experienced a large number of wildfires, which in turn increased the amount of biomass burning aerosols that reached the city. May 2019 was severely hit by regional wildfires (Fig. S7†) that affected almost 640 thousand hectares,[95] and raised the AAE mean to 1.57 ± 0.25 during the peak of the episode on May 5–15 with an hourly maximum of 2.52 on May 14 (Fig. S8†). However, our measurements yielded lower values all year round than values for the whole atmospheric column reported by a sun photometer of the Aerosol Robotic NETwork (AERONET) placed on the southwest of the city from 1999 to 2014 (1.50 ± 0.16 in the 440–870 nm range).[36]

The AAE showed a distinctive diurnal pattern all year round with clear magnitude differences between climatological seasons (Fig. 2f). The dry-warm season showed the largest values along the diurnal cycle, and the rainy season the lowest. Nighttime values during the dry-cool season were similar to those of the dry-warm season, and somewhat lower during the rest of the day. The advection of regional biomass burning plumes in concert with an intense irradiance and vigorous evolution of the boundary layer during the dry-warm season boosted the photochemical production of secondary aerosols, which in turn increased the AAE value during daytime. The low values observed during the morning rush hour reflect the higher absorption capacity of the traffic exhaust particles that dominate the aerosol burden at that time of the day.

3.5 Light absorption for black carbon and brown carbon

Throughout the diurnal cycle, both $b_{abs,BC,370}$ and $b_{abs,BrC,370}$ showed similar patterns and variabilities, but the former was consistently 3–4 times higher as shown in Fig. 3. Both coefficients followed the pattern observed for CO and NO_X, suggesting an important contribution from traffic emissions. The coefficient for BC showed a stronger correlation with both pollutant gases ($r^2 = 0.65$ and 0.71, respectively) than for BrC ($r^2 = 0.32$ and 0.31, respectively), suggesting BrC contributions from sources other than fossil fuel combustion, and a non-constant BrC to BC ratio during the diurnal course as a consequence of evolving photochemical processes and traffic patterns.

The diurnal patterns displayed by $b_{abs,BC,370}$ and $b_{abs,BrC,370}$ across the climatological seasons are unsurprisingly consistent with those already described for the net $b_{abs,370}$ and $b_{abs,880}$, respectively (see Fig. 2). The absorption coefficient for BC and BrC at 370 nm averaged 19.7 [2.1] and 5.6 [2.1] Mm^{-1}, respectively, during the two-year study. The highest means were recorded during the dry-cool season, 25.7 [2.1] and 7.7 [2.0] Mm^{-1}, followed by those during the dry-warm season, 20.6 [2.0] and 6.5 [2.1] Mm^{-1}, and finally by those during the rainy season, 15.6 [2.0] and 4.1 [1.9], respectively. The Mood's nonparametric test showed significant differences ($p < 0.05$) in the median values among seasons. However, no significant difference was observed in the fractional contribution of BrC to the net light absorption ($b_{abs,BrC,370}/b_{abs,370}$) during the dry-warm and dry-cool seasons, with contributions of 24% and 23%, respectively (Fig. 3c). The contribution decreased somewhat to 21% during the rainy season. Recent studies have reported contributions of 6–46% in cities of China and Korea.[15,16,96–98]

In summary, BrC and BC contribute 22% and 78% to the total light absorption in Mexico City, respectively. The BrC value corresponds to an increase of 28% on top of that attributed to BC in the 370 nm wavelength. This increase can be up to 32% during the dry-warm season; an increase of 40% had been previously estimated for this season using data from two intensive field campaigns in 2003 and 2006.[32]

3.6 Correlation of light absorption by BrC with NR-PM_1 components

The ACMS measurements covered a period of six months, including two months of the dry-cool season, a full dry-warm season, and one month of the rainy season. The NR-PM_1

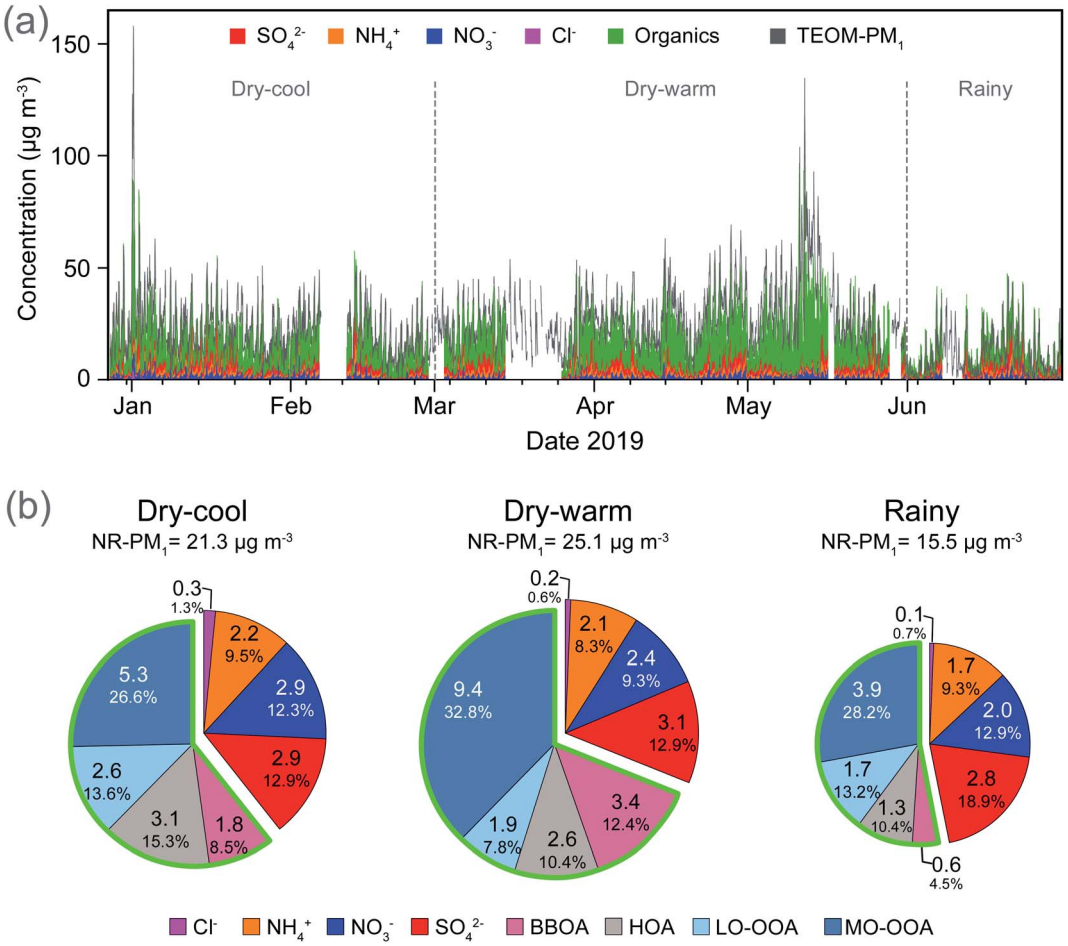

Fig. 4 Mass concentration of speciated non-refractory submicron particles and organic groups deconvolved by PMF. The time series by species include the PM_1 concentrations measured by TEOM as reference. The green contour in the pie charts groups the factors of organic aerosols determined by the PMF analysis.

Table 2 Coefficients of determination (r^2) between $b_{abs,BrC,370}$ and each group of organic aerosols as measured and resolved by ACSM and PMF. The OA is the assemble of the four groups and represents the total non-refractory organic fraction

Organic aerosol group	Full ACMS measurement period (December 2018–June 2019)	Dry-cool season (December 2018–February 2019)	Dry-warm season (March–May 2019)	Rainy season (June 2019)	Regional wildfires (April–May 2019)
OA	0.70	0.52	0.77	0.29	0.80
BBOA	0.68	0.40	0.80	0.11	0.84
MO-OOA	0.10	0.01	0.08	0.13	0.09
LO-OOA	0.33	0.28	0.45	0.19	0.51
HOA	0.37	0.65	0.29	0.41	0.31
BBOA + HOA	0.84	0.69	0.88	0.40	0.90

fraction represented 86% of the total PM_1 as measured by TEOM, while including eBC the contribution increased to 97%. The 3% gap corresponds to both uncounted species such as heavy metals and crustal elements and inherent measurement errors. The average concentration of organic aerosols accounted for 62% of NR-PM_1, SO_4^{2-} 15%, NO_3^- 12%, NH_4^+ 10% and Cl^- 1%. Four factors were identified from the PMF analysis of the organic fraction: MO-OOA, LO-OOA, HOA and BBOA. Among the organics, MO-OOA was the most abundant factor contributing 49% to the organic mass, followed by HOA (21%), LO-OOA (15%) and BBOA (15%). The time series and mass-fractional contributions of individual NR-PM_1 species and PMF factors are shown in Fig. 4. Similarly, Fig. S9† shows the time series of the OA mass loadings for each group together with the BC and BrC light absorption coefficients.

The total mass load of non-refractory OA showed a strong correlation with $b_{abs,BrC,370}$ ($r^2 = 0.70$), with an important variability between climatological seasons (see Table 2). In contrast,

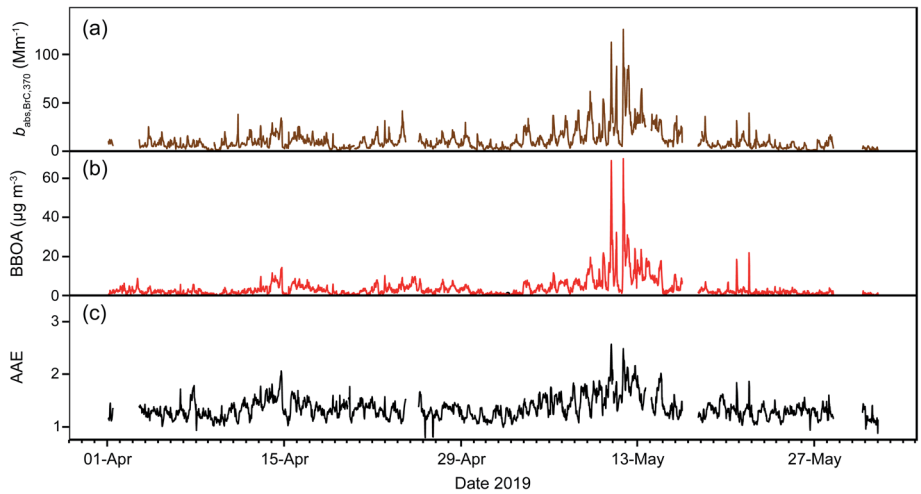

Fig. 5 Time series of (a) $b_{abs,BrC,370}$, (b) BBOA mass concentration and (c) AAE during the two months (April–May) of the dry-warm season of 2019 severely affected by regional wildfires across the central region of Mexico.

the other non-refractory ions (*i.e.*, NO_3^-, NH_4^+, SO_4^{2-} and Cl^-) showed poor correlations ($r^2 \leq 0.16$). Each group of organic aerosols as resolved by PMF yielded different coefficients of determination against $b_{abs,BrC,370}$, exposing the relevance of the aerosols' chemical composition and age in their ability to absorb light.

As expected, the mass loading of HOA yielded strong correlations against pollutant species associated with vehicular traffic, such as eBC, CO and NO_X ($r^2 > 0.60$), as well as $b_{abs,BC,370}$ ($r^2 = 0.72$). In contrast, the correlation against $b_{abs,BrC,370}$ was moderate ($r^2 = 0.37$), except during the dry-cool season ($r^2 = 0.65$), when as already indicated, a shallower boundary layer, increased atmospheric stability, and frequent thermal inversions enhanced the accumulation of pollutants. The highest abundance, as well as relative contribution of HOA to the total fraction of OA (26% on average) were observed in this season.

Plumes originating from wildfires and advected over Mexico City increased the contribution of BBOA in the total burden of OA to 19% during the dry-warm season. Biomass burning aerosols are an important source of BrC because numerous molecular chromophores make them efficient light absorbers at short wavelengths.[99] During the six-month period evaluated in this study we found a high correlation between BBOA and $b_{abs,BrC,370}$ ($r^2 = 0.68$) that strengthened during the dry-warm season ($r^2 = 0.80$), and even more during the peak of the regional wildfires ($r^2 = 0.84$). Null correlations were observed between BBOA and AAE, except during the dry-warm season ($r^2 = 0.40$). The enhancement of BBOA and their impact on $b_{abs,BrC,370}$ and AAE can be seen in the time series window for April and May 2019 shown in Fig. 5.

The light absorption in Mexico City is therefore modulated by the presence of BBOA and HOA. The mass loading of both

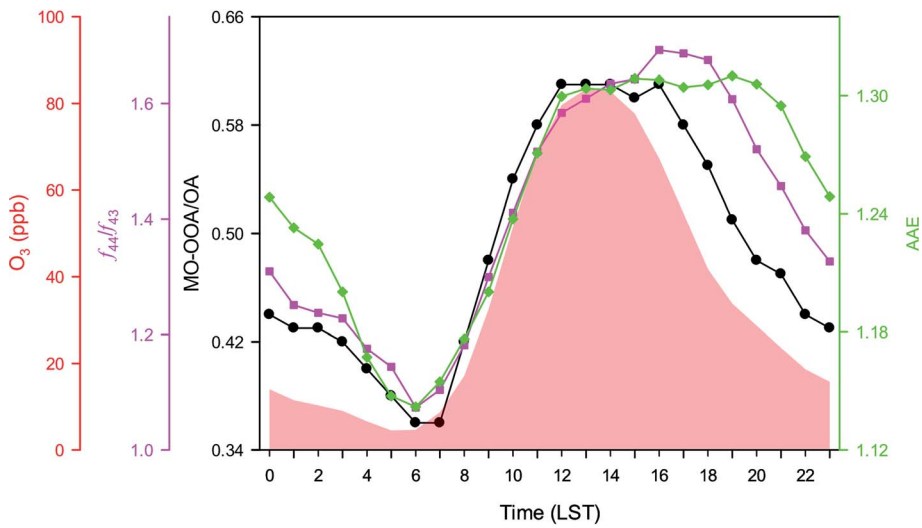

Fig. 6 Diurnal variability of the ambient concentration of O_3 (red shaded area), degree of oxidation obtained as the ratio between ions *m/z* 44 and 43 (f_{44}/f_{43}) measured by ACMS, MO-OOA organic mass fraction (MO-OOA/OA), and absorption Ångström exponent (AAE).

Table 3 Mass-normalized absorption efficiency (MAE) and percentage contribution to the total BrC light absorption at 370 nm for each group of organic aerosols derived from the PMF analysis during the six-month period of ACSM measurements. The intercepts and correlation coefficients of the least-square linear regression used to obtain $b_{abs,BrC}$ based on the estimated MAEs (eqn (6)) against the approach based on the difference between the total aerosol absorption and the absorptions related to BC (eqn (3)) are also included. The numbers at the right of the ± symbol indicate one standard deviation and give an idea of the day-to-day variability

Group of organic aerosols	Dry-warm (March–May 2019)	Rainy (June 2019)	Dry-cool (December 2018–February 2019)	Full period (December 2018–June 2019)
BBOA ($m^2\ g^{-1}$)	1.82 ± 0.02 (55%)	0.40 ± 0.14 (6%)	0.83 ± 0.09 (14%)	1.73 ± 0.02 (43%)
HOA ($m^2\ g^{-1}$)	1.76 ± 0.03 (40%)	1.47 ± 0.07 (49%)	1.79 ± 0.03 (53%)	1.75 ± 0.02 (46%)
LO-OOA ($m^2\ g^{-1}$)	0.01 ± 0.04 (0.2%)[a]	0.03 ± 0.06 (1%)[a]	0.97 ± 0.06 (24%)	0.29 ± 0.03 (6%)
MO-OOA ($m^2\ g^{-1}$)	0.00 ± 0.01 (0%)[a]	0.04 ± 0.03 (4%)[a]	−0.14 ± 0.02 (−7%)[a]	−0.00 ± 0.01 (0%)[a]
Intercept (Mm^{-1})	0.73 ± 0.12	1.51 ± 0.12	1.33 ± 0.17	0.76 ± 0.10
r^2	0.89	0.45	0.74	0.86

[a] Estimated values were statistically not different from zero for a significance level of 5%.

components together (*i.e.*, BBOA + HOA) strengthened the correlation with $b_{abs,BrC,370}$ up to 0.90 during both, dry-warm and dry-cool seasons. In other words, vehicular traffic is the main local contributor on a daily basis, while biomass burning becomes the major contributor during the dry-warm season affected by wildfires in surrounding regions.

Relative to SOA, MO-OOA represented almost half of the load of OA. The high contribution of MO-OOA to the total OA mass did not directly increase the absorption of light; neither had a relevant contribution to BrC, but its diurnal evolution apparently modulated the aerosols efficiency to absorb light. The absorption Ångström exponent and the MO-OOA fraction within the OA burden (*i.e.*, MO-OOA/OA) followed similar patterns along the diurnal cycle; after sunrise both increased at the same rate and peaked simultaneously. Browne *et al.*[100] observed that the oxidation of biomass burning aerosols by O_3 lessens light absorption at longer wavelengths, but not at shorter wavelengths, increasing AAE as result. This partial bleaching occurs relatively fast (minutes to hours) at moderate or high O_3 concentrations due to an oxidative degradation of the chromophores absorbing at longer wavelengths. Then the oxidation process is driven by the hydroxyl radical (OH), becoming less absorbing with age, decreasing AAE.[99,100] This mechanism of heterogenous oxidation becomes important in cites affected by O_3 pollution, like Mexico City, where over 200 days per year report hourly concentrations >95 ppb (**https://www.aire.cdmx.gob.mx**).

We use the ratio between the ions *m/z* 44 and 43 (f_{44}/f_{43}) measured by ACMS to further investigate the effect of chemical aging on the optical properties of BrC. This ratio defines the degree of oxidation of the organic fraction.[101,102] Highly aged aerosols are represented by f_{44} (CO_2^+, likely from acid groups), and less aged aerosols by f_{43} (mostly $C_2H_3O^+$ from non-acid oxygenates, and $C_3H_7^+$ from alkyl groups). The MO-OOA spectra depict higher f_{44} and lower f_{43} than the LO-OOA spectra, thus higher ratios indicate older particles, chemically speaking. However, the f_{44}/f_{43} ratio suggests a longer oxidation period in the afternoon when compared to the MO-OOA organic mass fraction (Fig. 6). The relative abundance of MO-OOA peaked at noon, and remained constant until midafternoon (16 h), when it started to decrease as a consequence of a major contribution of freshly emitted particles; but interestingly that was when the f_{44}/f_{43} ratio reached a maximum value. The load of highly oxidated aerosols started to decrease until two hours later (18 h), but it was only after sunset (20 h) when the ability of the particles to absorb light began to increase (*i.e.*, AAE started to drop). The chemical aging of the particles declined throughout the night, reaching minimum values the f_{44}/f_{43} ratio, the MO-OOA/OA, and AAE before sunrise (6 h). The strong photochemical activity depicted by the rapid increase of O_3 throughout the morning (6–12 h) was also evident in the increase of oxidated aerosols, which in turn drastically slowed down the ability of the particles to absorb light.

The complex mixture of urban aerosols and wide range of aging processes, in which the rapid heterogeneous oxidation by O_3 apparently prevails over a slower OH oxidation, except during stagnation episodes, act together to alter the BrC optical properties in the atmosphere of Mexico City. Residence times of air masses in the basin are relatively short (~12 h) with little carry-over from day to day and little recirculation.[103]

3.7 Mass absorption apportionment by type of organic aerosol

The MAE for each OA factor as defined by PMF, was obtained from the model described by eqn (6). The unconstrained application of this model was able to capture 86% of the $b_{abs,BrC,370}$ variance for the full study period, and demonstrated that the OA factors are good predictors to assess the light absorption by BrC in Mexico City. Table 3 shows the resulting MAE for each group of OA. The regression's intercepts and correlation coefficients, also shown in Table 3, indicate the variability not explained by the model to calculate $b_{abs,BrC,370}$ using as reference the BrC absorption obtained from the approach based on the difference between the total aerosol absorption and the absorptions related to BC, (eqn (3)).

The individual MAE showed distinctive values across seasons. BBOA and HOA returned the highest coefficients. As expected, the highest coefficients for BBOA were observed during the dry-warm season, and the lowest during the rainy

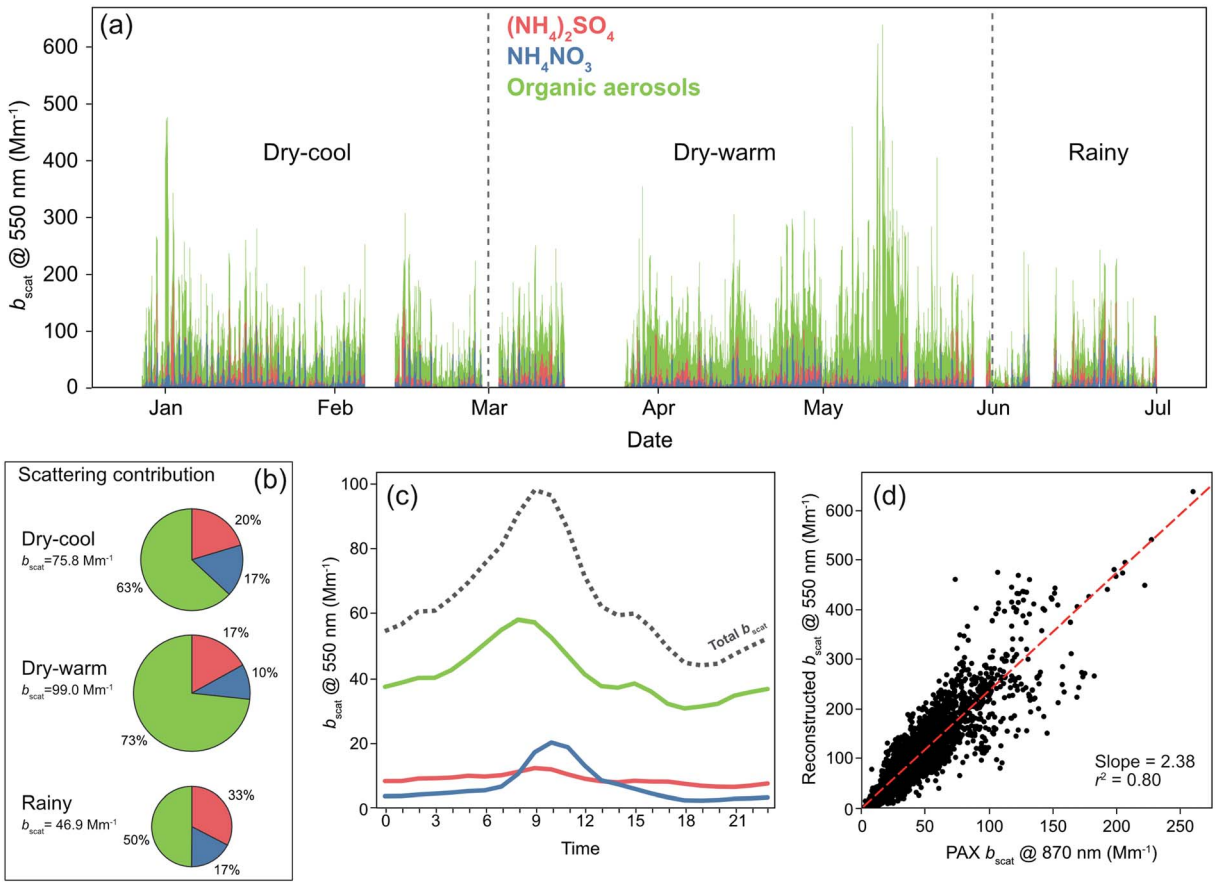

Fig. 7 (a) Time series of light-scattering coefficients at 550 nm ($b_{scat,550}$) obtained by the revised US-EPA IMPROVE equation for each aerosol component identified by the proposed ion pairing scheme during the sampling campaign of 2019. (b) Contributions of each aerosol component to total scattering by climatological season. (c) Diurnal variability of the individual coefficients based on geometric means, the dashed line corresponds to their sum. (d) Regression plot between the reconstructed b_{scat} at 550 nm, and b_{scat} at 870 nm measured by PAX.

season due to the absence of regional wildfires. The coefficients for HOA did not vary substantially across seasons, contrary to the coefficients for LO-OOA, which yielded values statistically equal to zero during the dry-warm and rainy seasons. MO-OOA registered consistently the lowest coefficients, even coefficients with negative values, during the dry-cool season due to the unconstrained application of the model. This finding, like our previous results, highlights the weak contribution of highly oxidized OA to light-absorbtion.

The MAE obtained for BBOA should be taken with caution since the values estimated in this study varied from season to season. The regional landscape is quite heterogeneous, and therefore different types of wildfires can be expected with a complex variability of emissions in terms of origin, chemical characterization, emission rates, plume characteristics and age, and transport patterns relying on synoptic scale meteorology.[104–106] In the absence of wildfires, BBOA can be related to the local burning of trash and the use of biomass as fuel for cooking by many street-food stalls across the city.[41,80]

The MAEs reported in this study are within those found in urban areas of different characteristics. For example, a coefficient of 1.67 $m^2\ g^{-1}$ at 637 nm for HOA was reported for traffic related sources in Barcelona, Spain,[107] while coefficients ranging from 1.34 to 2.04 $m^2\ g^{-1}$ at 365–370 nm were reported for Kanpur, India,[14] Yangzhou, China,[108] and Manaus, Brazil.[17] With respect to BBOA, like in our case, a wide variability has been observed in other places depending on the presence of biomass burning and the plumes' age.[97]

In terms of individual contributions to $b_{abs,BrC}$ at 370 nm obtained from the product of MAE and concentration by group of OA, HOA was the dominant group during the dry-cool and rainy seasons with contributions of 53% and 49%, respectively. BBOA dominated the light absorption during the dry-warm season with 55%, but contributed only 6% during the rainy season. LO-OOA contributed 24% during the dry-cool season, and almost zero during the other two seasons. Negligible contributions from MO-OOA were observed along the three seasons due to the presence of highly oxidized non-absorbing species, including oxidized chromophores that inhibit the aerosols absorption capacity as observed in similar studies.[14,97]

3.8 Light scattering reconstruction

The application of the modified ion pairing scheme (eqn (8)) to approximate the concentrations of inorganic compounds obtained from the ACMS measurements showed that the

inorganic fraction was dominated by $(NH_4)_2SO_4$, NH_4NO_3 and NH_4Cl, while H_2SO_4 was not identified and NH_4HSO_4 was absent most of the time. The mass loadings of the former two compounds and the loading of the total organic fraction were used to reconstruct the light-scattering coefficient at 550 nm applying the revised US-EPA IMPROVE equation (eqn (7)). The time series of $b_{scat,550}$ with the apportionment of each aerosol component are shown in Fig. 7. The geometric mean obtained by this approach returned a $b_{scat,550} = 82.1\ [2.2]\ Mm^{-1}$. A strong correlation against the b_{scat} PAX measurements at 870 nm was found ($r^2 = 0.80$).

The organic fraction dominated light scattering with a contribution of 68%. Ammonium sulfate contributed 19%, and NH_4NO_3 13% across the six-month sampling period. Fig. 7 shows the contributions for each climatological season. The larger contribution of organic aerosols during the dry-warm season responded to more frequent biomass burning plumes full of aged particles reaching the city, while the lower contributions portrayed by NH_4NO_3 responded to an increased volatility under warmer conditions. The scattering coefficient for $(NH_4)_2SO_4$ did not vary essentially between seasons, suggesting a constant flux of SO_2 within and outside the city.

As depicted in Fig. 7c, the morning peak in the total $b_{scat,550}$ responded to the mix of fresh and aged organic aerosols, while the contribution of NH_4NO_3 became evident after sunrise as a consequence of the photochemical activity kick off. The total light scattering peaked at 9–10 h, then experienced a small decrease during the next two hours and remained relatively constant in the early afternoon because of a slight increase of organic aerosols and a slower depletion rate of NH_4NO_3. Ammonium sulfate showed a high background contribution with a slight morning increase. Previous studies in Mexico City reported a similar diurnal pattern of light scattering.[29,31]

4. Summary and conclusions

A net light aerosol extinction of 31.6 [1.9] Mm^{-1} in the near infrared spectral region was observed during a two-year study (2017–2019) in Mexico City. Depending on the climatological season, 65–74% was attributed to light scattering. During the dry-warm season (February to May) ubiquitous regional wildfires increased the burden of high-scattering and high-absorbing aerosols. On regular days (*i.e.*, not affected by wildfire plumes), emissions from vehicular traffic were the driver of aerosol light extinction. Emissions from cooking and domestic heating, as well as from industrial activities apparently had minor contributions. The light scattering and absorption coefficients observed in this study are similar to those reported in the literature for urban atmospheres highly impacted by traffic pollution, but lower than those impacted by woodsmoke.

The organic fraction of aerosols dominated both the submicron mass loading, as measured by mass spectroscopy of non-refractory components, and light scattering. At least half of the light scattering can be attributed to organic aerosols during regular days, and over 80% during wildfire episodes. Nitrates and sulfates are also important light scattering contributors. The former has a larger contribution on regular days (20%) than during the wildfire season (14%), the opposite is true for the latter (11% and 22%, respectively).

The light absorption coefficients showed distinctive seasonal power law distributions as a function of wavelength. The biomass burning plumes rich in organic aerosols reduced somewhat the coefficients of light absorption, but because of their abundance, the biomass burning aerosols exceeded over 50% of the organic contribution to light absorption at 370 nm during the dry-warm season. The hydrocarbon-like organic aerosols strongly related to vehicular traffic were the dominant contributors (~50%) in the absence of biomass burning plumes. Interestingly, the abundance of aged organic aerosols with an important regional character, represented by the MO-OOA group, had a null contribution during the three climatological seasons due to the presence of highly oxidized non-absorbing species. However, less aged organic aerosols associated with local chemical processes, represented by the LO-OOA group, showed a contribution of 24% in periods not affected by biomass burning. These results indicate that vehicular traffic is the main contributor of light absorption on a daily basis by the direct emission of black carbon and organic aerosols, and indirect participation in the production of secondary organic aerosols through the emission of precursor species, while biomass burning is the major contributor during the wildfires season.

A strong correlation ($r^2 > 0.70$) between the light absorption coefficients for brown carbon and the total organic aerosol mass loadings helps to explain the additional light absorption from carbonaceous aerosols other than black carbon. Brown carbon added on average 5.6 [2.1] Mm^{-1} to the absorption of 19.7 [2.1] Mm^{-1} related only to black carbon at 370 nm, which represents an additional 28%, that can be higher during wildfire episodes, *e.g.*, during the episode of April–May 2019 the light absorption was 40% of that attributed to black carbon.

A comprehensive characterization of the aerosol optical properties is fundamental to design effective emission control policies to improve air quality and mitigate climate change. The results presented in this study provide information to assess the visibility deterioration within the city, which despite being the most evident effect of air pollution, has not received the necessary attention from environmental authorities. In the same way, the diurnal and seasonal variations of the optical properties and chemical composition of the atmospheric aerosols provide essential information to improve the retrieval of AOD from satellite and ground-based measurements over Mexico City and surrounding regions all year round. An accurate interpretation of the AOD will help to address the radiative forcing and air pollution related to seasonal wildfires, as well as to evaluate the regional impact caused by the urban plume of smoke. At the city scale, the impact of brown carbon and its associated optical properties on atmospheric chemistry and micrometeorology must be considered to update current air quality and climate change programs.

Author contributions

AR: Conceptualization, Methodology, Investigation, Data curation, Formal analysis, Writing-original draft. EV:

Conceptualization, Formal analysis, Writing-original draft. MR: Investigation, Data curation, Writing-review and editing. GA: Methodology, Investigation, Writing-review and editing. OR: Conceptualization, Project administration, Writing-review.

Conflicts of interest

There are no conflicts of interest to declare.

Acknowledgements

We acknowledge the data provided by the Mexico City's Secretariat for the Environment (SEDEMA). The authors acknowledge the assistance provided by the staff of the Environmental Analysis Laboratory. The support provided by M. Sánchez-Rodríguez, A. Neria-Hernández, O. Hernández-Castillo and A. López-Medina was fundamental to operate the instruments satisfactorily. No funding was provided for the data analysis and manuscript preparation. The opinions set forth in this article are those of the authors and do not necessarily represent the official position of SEDEMA. The editorial assistance and suggestions of Luisa T. Molina (Molina Center for Energy and the Environment) are also greatly appreciated. The authors want to thank the editor and the anonymous reviewers for their comments, which helped improved the initially submitted version.

References

1 J. H. Seinfeld and S. N. Pandis, *Atmospheric Chemistry and Physics: from Air Pollution to Climate Change*, John Wiley & Sons, Hoboken, NJ, 3rd edn, 2016, pp.633–638.

2 P. Laj, J. Klausen, M. Bilde, C. Plass-Duelmer, G. Pappalardo, C. Clerbaux, U. Baltensperger, J. Hjorth, D. Simpson, S. Reimann, P. F. Coheur, A. Richter, M. De Maziere, Y. Rudich, G. McFiggans, K. Torseth, A. Wiedensohler, S. Morin, M. Schulz, J. D. Allan, J. L. Attie, I. Barnes, W. Birmili, J. P. Cammas, J. Dommen, H. P. Dorn, D. Fowler, S. Fuzzi, M. Glasius, C. Granier, M. Hermann, I. S. A. Isaksen, S. Kinne, I. Koren, F. Madonna, M. Maione, A. Massling, O. Moehler, L. Mona, P. S. Monks, D. Muller, T. Muller, J. Orphal, V. H. Peuch, F. Stratmann, D. Tanre, G. Tyndall, A. A. Riziq, Van M. Roozendael, P. Villani, B. Wehner, H. Wex and A. A. Zardini, Measuring atmospheric composition change, *Atmos. Environ.*, 2009, **43**, 5351–5414.

3 A. Laskin, J. Laskin and S. A. Nizkorodov, Chemistry of atmospheric brown carbon, *Chem. Rev.*, 2015, **115**(10), 4335–4382.

4 A. J. Prenni, J. L. Hand, W. C. Malm, S. Copeland, G. Luo, F. Yu, N. Taylor, L. M. Russell and B. A. Schichtel, An examination of the algorithm for estimating light extinction from IMPROVE particle speciation data, *Atmos. Environ.*, 2019, **214**, 116880.

5 H. Moosmüller, R. K. Chakrabarty and W. P. Arnott, Aerosol light absorption and its measurement: a review, *J. Quant. Spectrosc. Radiat. Transf.*, 2009, **110**(11), 844–878.

6 A. Petzold, J. A. Ogren, M. Fiebig, P. Laj, S.-M. Li, U. Baltensperger, T. Holzer-Popp, S. Kinne, G. Pappalardo, N. Sugimoto, C. Wehrli, A. Wiedensohler and X.-Y. Zhang, Recommendations for reporting "black carbon" measurements, *Atmos. Chem. Phys.*, 2013, **13**, 8365–8379.

7 M. O. Andreae and A. Gelencsér, Black carbon or brown carbon? The nature of light-absorbing carbonaceous aerosols, *Atmos. Chem. Phys.*, 2006, **6**, 3131–3148.

8 M. Pósfai, A. Gelencsér, R. Simonics, K. Arató, J. Li, P. V. Hobbs and P. R. Buseck, Atmospheric tar balls: particles from biomass and biofuel burning, *J. Geophys. Res. Atmos.*, 2004, **109**(D6), 06213.

9 A. Hoffer, A. Gelencsér, P. Guyon, G. Kiss, O. Schmid, G. P. Frank, P. Artaxo and M. O. Andreae, Optical properties of humic-like substances (HULIS) in biomass-burning aerosols, *Atmos. Chem. Phys.*, 2006, **6**, 3563–3570.

10 J. Yan, X. Wang, P. Gong, C. Wang and Z. Cong, Review of brown carbon aerosols: recent progress and perspectives, *Sci. Total Environ.*, 2018, **634**, 1475–1485.

11 A. J. Ding, X. Huang, W. Nie, J. N. Sun, V. M. Kerminen, T. Petäjä, H. Su, Y. F. Cheng, X. Q. Yang, M. H. Wang and X. G. Chi, Enhanced haze pollution by black carbon in megacities in China, *Geophys. Res. Lett.*, 2016, **43**(6), 2873–2879.

12 Y. Yang, Z. Zheng, S. Y. Yim, M. Roth, G. Ren, Z. Gao, T. Wang, Q. Li, C. Shi, G. Ning and Y. Li, PM2.5 pollution modulates wintertime urban heat island intensity in the Beijing-Tianjin-Hebei Megalopolis, China, *Geophys. Res. Lett.*, 2020, **47**(1), e2019GL084288.

13 A. Ipiña, G. López-Padilla, A. Retama, R. D. Piacentini and S. Madronich, Ultraviolet radiation environment of a tropical megacity in transition: Mexico City 2000–2019, *Environ. Sci. Technol.*, 2021, **55**(16), 10946–10956.

14 R. Satish, P. Shamjad, N. Thamban, S. Tripathi and N. Rastogi, Temporal Characteristics of Brown Carbon over the Central Indo-Gangetic Plain, *Environ. Sci. Technol.*, 2017, **51**(12), 6765–6772.

15 S. Park, S. C. Son and S. Lee, Characterization, sources, and light absorption of fine organic aerosols during summer and winter at an urban site, *Atmos. Res.*, 2018, **213**, 370–380.

16 J. Wang, W. Nie, Y. Cheng, Y. Shen, X. Chi, J. Wang, X. Huang, Y. Xie, P. Sun, Z. Xu, X. Qi, H. Su and A. Ding, Light absorption of brown carbon in eastern China based on 3-year multi-wavelength aerosol optical property observations and an improved absorption Ångström exponent segregation method, *Atmos. Chem. Phys.*, 2018, **18**, 9061–9074, DOI: 10.5194/acp-18-9061-2018.

17 S. S. de Sá, L. V. Rizzo, B. B. Palm, P. Campuzano-Jost, D. A. Day, L. D. Yee, R. Wernis, G. Isaacman-VanWertz, J. Brito, S. Carbone, Y. J. Liu, A. Sedlacek, S. Springston, A. H. Goldstein, H. M. J. Barbosa, M. L. Alexander, P. Artaxo, J. L. Jimenez and S. T. Martin, Contributions of biomass-burning, urban, and biogenic emissions to the concentrations and light-absorbing properties of particulate matter in central Amazonia during the dry season, *Atmos. Chem. Phys.*, 2019, **19**, 7973–8001.

18 J. M. Rincón-Riveros, M. A. Rincón-Caro, A. P. Sullivan, J. F. Mendez-Espinosa, L. C. Belalcazar, M. Quirama Aguilar and R. Morales Betancourt, Long-term brown carbon and smoke tracer observations in Bogotá, Colombia: association with medium-range transport of biomass burning plumes, *Atmos. Chem. Phys.*, 2020, **20**, 7459–7472.

19 A. D. de Almeida Castanho, R. Prinn, V. Martins, M. Herold, C. Ichoku and L. T. Molina, Analysis of Visible/SWIR surface reflectance ratios for aerosol retrievals from satellite in Mexico City urban area, *Atmos. Chem. Phys.*, 2007, **7**, 5467–5477.

20 J. C. Doran, S. Abbott, J. Archuleta, X. Bian, J. Chow, R. L. Coulter, S. F. J. De Wekker, S. Edgerton, S. Elliott, A. Fernandez and J. D. Fast, The IMADA-AVER boundary layer experiment in the Mexico City area, *Bull. Am. Meteorol. Soc.*, 1998, **79**(11), 2497–2508.

21 S. A. Edgerton, X. Bian, J. C. Doran, J. D. Fast, J. M. Hubbe, E. L. Malone, W. J. Shaw, C. D. Whiteman, S. Zhong, J. L. Arriaga, E. Ortiz, M. Ruiz, G. Sosa, E. Vega, T. Limon, F. Guzman, J. Archuleta, J. E. Bossert, S. Elliot, J. T. Lee, L. A. McNair, J. C. Chow, J. G. Watson, R. L. Coulter, P. V. Doskey, J. S. Gaffney, N. A. Marley, W. Neff and R. Petty, Particulate Air pollution in Mexico City: A Collaborative Research Project, *J. Air Waste Manag. Assoc.*, 1999, **49**, 1221–1229.

22 J. C. Chow, J. G. Watson, S. A. Edgerton and E. Vega, Chemical composition of $PM_{2.5}$ and PM_{10} in Mexico City during winter 1997, *Sci. Total Environ.*, 2002, **287**, 177–201.

23 D. Salcedo, T. B. Onasch, K. Dzepina, M. R. Canagaratna, Q. Zhang, J. A. Huffman, P. F. DeCarlo, J. T. Jayne, P. Mortimer, D. R. Worsnop, C. E. Kolb, K. S. Johnson, B. Zuberi, L. C. Marr, R. Volkamer, R. L. T. Molina, M. J. Molina, B. Cardenas, R. M. Bernabé, C. Márquez, J. S. Gaffney, N. A. Marley, A. Laskin, V. Shutthanandan, Y. Xie, W. Brune, R. Lesher, T. Shirley and J. L. Jimenez, Characterization of ambient aerosols in Mexico City during the MCMA-2003 campaign with Aerosol Mass Spectrometry: results from the CENICA Supersite, *Atmos. Chem. Phys.*, 2006, **6**, 925–946.

24 L. T. Molina, C. E. Kolb, B. de Foy, B. K. Lamb, W. H. Brune, J. L. Jimenez, R. Ramos-Villegas, J. Sarmiento, V. H. Paramo-Figueroa, B. Cardenas, V. Gutierrez-Avedoy and M. J. Molina, Air quality in North America's most populous city – overview of the MCMA-2003 campaign, *Atmos. Chem. Phys.*, 2007, **7**, 2447–2473.

25 L. T. Molina, S. Madronich, J. S. Gaffney, E. Apel, B. de Foy, J. Fast, R. Ferrare, S. Herndon, J. L. Jimenez, B. Lamb, A. R. Osornio-Vargas, P. Russell, J. J. Schauer, P. S. Stevens, R. Volkamer and M. Zavala, An overview of the MILAGRO 2006 Campaign: Mexico City emissions and their transport and transformation, *Atmos. Chem. Phys.*, 2010, **10**, 8697–8760.

26 J. C. Doran, J. C. Barnard, W. P. Arnott, R. Cary, R. Coulter, J. D. Fast, E. I. Kassianov, L. Kleinman, N. S. Laulainen, T. Martin, G. Paredes-Miranda, M. S. Pekour, W. J. Shaw, D. F. Smith, S. R. Springston and X.-Y. Yu, The T1-T2 study: evolution of aerosol properties downwind of Mexico City, *Atmos. Chem. Phys.*, 2007, **7**, 1585–1598.

27 A. C. Aiken, D. Salcedo, M. J. Cubison, J. A. Huffman, P. F. DeCarlo, I. M. Ulbrich, K. S. Docherty, D. Sueper, J. R. Kimmel, D. R. Worsnop, A. Trimborn, M. Northway, E. A. Stone, J. J. Schauer, R. M. Volkamer, E. Fortner, B. de Foy, J. Wang, A. Laskin, V. Shutthanandan, J. Zheng, R. Zhang, J. Gaffney, N. A. Marley, G. Paredes-Miranda, W. P. Arnott, L. T. Molina, G. Sosa and J. L. Jimenez, Mexico City aerosol analysis during MILAGRO using high resolution aerosol mass spectrometry at the urban supersite (T0) – Part 1: fine particle composition and organic source apportionment, *Atmos. Chem. Phys.*, 2009, **9**, 6633–6653.

28 D. Baumgardner, G. L. Kok and G. B. Raga, On the diurnal variability of particle properties related to light absorbing carbon in Mexico City, *Atmos. Chem. Phys.*, 2007, **7**, 2517–2526.

29 N. A. Marley, J. S. Gaffney, T. Castro, A. Salcido and J. Frederick, Measurements of aerosol absorption and scattering in the Mexico City Metropolitan Area during the MILAGRO field campaign: a comparison of results from the T0 and T1 sites, *Atmos. Chem. Phys.*, 2009, **9**, 189–206.

30 N. A. Marley, J. S. Gaffney, M. Tackett, N. C. Sturchio, L. Heraty, N. Martinez, K. D. Hardy, A. Marchany-Rivera, T. Guilderson, A. MacMillan and K. Steelman, The impact of biogenic carbon sources on aerosol absorption in Mexico City, *Atmos. Chem. Phys.*, 2009b, **9**, 1537–1549.

31 G. Paredes-Miranda, W. P. Arnott, J. L. Jimenez, A. C. Aiken, J. S. Gaffney and N. A. Marley, Primary and secondary contributions to aerosol light scattering and absorption in Mexico City during the MILAGRO 2006 campaign, *Atmos. Chem. Phys.*, 2009, **9**, 3721–3730.

32 J. C. Barnard, R. Volkamer and E. I. Kassianov, Estimation of the mass absorption cross section of the organic carbon component of aerosols in the Mexico City Metropolitan Area, *Atmos. Chem. Phys.*, 2008, **8**, 6665–6679.

33 G. Li, N. Bei, X. Tie and L. T. Molina, Aerosol effects on the photochemistry in Mexico City during MCMA-2006/MILAGRO campaign, *Atmos. Chem. Phys.*, 2011, **11**, 5169–5182.

34 A. Retama, D. Baumgardner, G. B. Raga, G. R. McMeeking and J. W. Walker, Seasonal and diurnal trends in black carbon properties and co-pollutants in Mexico City, *Atmos. Chem. Phys.*, 2015, **15**(16), 9693.

35 R. N. Liñán-Abanto, O. Peralta, D. Salcedo, L. G. Ruiz-Suárez, P. Arnott, G. Paredes-Miranda, H. Alvarez-Ospina and T. Castro, Optical properties of atmospheric particles over an urban site in Mexico City and a peri-urban site in Queretaro, *J. Atmos. Chem.*, 2019, **76**(3), 201–228.

36 G. Carabali, H. R. Estévez, M. Valdés-Barrón, R. Bonifaz-Alfonzo, D. Riveros-Rosas, V. M. Velasco-Herrera and F. A. Vázquez-Gálvez, Aerosol climatology over the Mexico City basin: characterization of optical properties, *Atmos. Res.*, 2017, **194**, 190–201.

37 G. I. Gorchakov, A. V. Karpov, A. V. Vasiliev and I. A. Gorchakova, Brown and black carbons in megacity smogs, *Atmos. Ocean. Opt.*, 2017, **30**(3), 248–254.
38 SEDEMA, Secretaría del Medio Ambiente de la Ciudad de México, *Calidad del aire en la Ciudad de México, informe 2017*, Mexico City, 2018, p. 21.
39 L. T. Molina, E. Velasco, A. Retama and M. Zavala, Experience from integrated air quality management in the Mexico City metropolitan area and Singapore, *Atmosphere*, 2019, **10**(9), 512.
40 R. Volkamer, J. L. Jimenez, F. San Martini, K. Dzepina, Q. Zhang, D. Salcedo, L. T. Molina, D. R. Worsnop and M. J. Molina, Secondary organic aerosol formation from anthropogenic air pollution: rapid and higher than expected, *Geophys. Res. Lett.*, 2006, **33**(17), L17811.
41 A. Retama, A. Neria-Hernández, M. Jaimes-Palomera, O. Rivera-Hernández, M. Sánchez-Rodríguez, A. López-Medina and E. Velasco, Fireworks: a major source of inorganic and organic aerosols during Christmas and New Year in Mexico City, *Atmos. Environ.: X*, 2019, **2**, 100013.
42 F. Guerrero, H. Álvarez-Ospina, A. Retama, A. López-Medina, T. Castro and D. Salcedo, Seasonal changes in the PM1 chemical composition north of Mexico City, *Atmósfera*, 2017, **30**(3), 243–258.
43 B. Ríos and G. B. Raga, Spatio-temporal distribution of burned areas by ecoregions in Mexico and Central America, *Int. J. Rem. Sens.*, 2018, **39**(4), 949–970.
44 DMT, Dropplet Measurement Technologies, *Photoacoustic Extinctiometer (PAX) Operator Manual DOC-0301 Revision B-3*, 2012, Boulder, CO.
45 L. Drinovec, G. Mocnik, P. Zotter, A. S. H. Prévôt, C. Ruckstuhl, E. Coz, M. Rupakheti, J. Sciare, T. Müller, A. Wiedensohler and A. D. A. Hansen, The "dual-spot" Aethalometer: an improved measurement of aerosol black carbon with real-time loading compensation, *Atmos. Meas. Tech.*, 2015, **8**, 1965–1979.
46 J. C. Corbin, S. M. Pieber, H. Czech, M. Zanatta, G. Jakobi, D. Massabò, J. Orasche, I. El Haddad, A. A. Mensah, B. Stengel, L. Drinovec, G. Mocnik, R. Zimmermann, A. S. H. Prévôt and M. Gysel, Brown and black carbon emitted by a marine engine operated on heavy fuel oil and distillate fuels: optical properties, size distributions and emission factors, *J. Geophys. Res. Atmos.*, 2018, **123**, 6175–6195.
47 N. K. Kumar, J. C. Corbin, E. A. Bruns, D. Massabó, J. G. Slowik, L. Drinovec, G. Močnik, P. Prati, A. Vlachou, U. Baltensperger, M. Gysel, I. El-Haddad and A. S. H. Prévôt, Production of particulate brown carbon during atmospheric aging of residential wood-burning emissions, *Atmos. Chem. Phys.*, 2018, **18**, 17843–17861.
48 E. Weingartner, H. Saathoff, M. Schnaiter, N. Streit, B. Bitnar and U. Baltensperger, Absorption of light by soot particles: determination of the absorption coefficient by means of aethalometers, *J. Aerosol Sci.*, 2003, **34**, 1445–1463.
49 J. R. Laing, D. A. Jaffe and A. J. Sedlacek III, Comparison of Filter-based Absorption Measurements of Biomass Burning Aerosol and Background Aerosol at the Mt. Bachelor Observatory, *Aerosol Air Qual. Res.*, 2020, **20**, 663–678.
50 D. M. Kalbermatter, G. Močnik, L. Drinovec, B. Visser, J. Röhrbein, M. Oscity, E. Weingartner, A.-P. Hyvärinen and K. Vasilatou, Comparing black-carbon- and aerosol-absorption-measuring instruments – a new system using lab-generated soot coated with controlled amounts of secondary organic matter, *Atmos. Meas. Tech.*, 2022, **15**, 561–572.
51 G. Zhao, Y. Yu, P. Tian, J. Li, S. Guo and C. Zhao, Evaluation and correction of the ambient particle spectral light absorption measured using a filter-based aethalometer, *Aerosol Air Qual. Res.*, 2020, 1833–1841.
52 Magee Scientific, **https://mageesci.com/tape/Magee_Scientific_Filter_Aethalometer_AE_Tape_Replacement_discussion.pdf**, accessed December 2021.
53 N. L. Ng, S. C. Herndon, A. Trimborn, M. R. Canagaratna, P. L. Croteau, T. B. Onasch, D. Sueper, D. R. Worsnop, Q. Zhang, Y. L. Sun and J. T. Jayne, An Aerosol Chemical Speciation Monitor (ACSM) for routine monitoring of the composition and mass concentrations of ambient aerosol, *Aerosol Sci. Tech.*, 2011, **45**, 780–794.
54 P. Paatero and U. Tapper, Positive matrix factorization: a non- negative factor model with optimal utilization of error estimates of data values, *Environmetrics*, 1994, **5**, 111–126.
55 I. M. Ulbrich, M. R. Canagaratna, Q. Zhang, D. R. Worsnop and J. L. Jimenez, Interpretation of organic components from Positive Matrix Factorization of aerosol mass spectrometric data, *Atmos. Chem. Phys.*, 2009, **9**, 2891–2918.
56 Y. Zhang, O. Favez, J.-E. Petit, F. Canonaco, F. Truong, N. Bonnaire, V. Crenn, T. Amodeo, A. S. H. Prévôt, J. Sciare, V. Gros and A. Albinet, Six-year source apportionment of submicron organic aerosols from near-continuous highly time-resolved measurements at SIRTA (Paris area, France), *Atmos. Chem. Phys.*, 2019, **19**, 14755–14776.
57 M. R. Alfarra, A. S. H. Prevot, S. Szidat, J. Sandradewi, S. Weimer, V. A. Lanz, D. Schreiber, M. Mohr and U. Baltensperger, Identification of the mass spectral signature of organic aerosols from wood burning emissions, *Environ. Sci. Technol.*, 2007, **41**(16), 5770–5777.
58 D. Fabbri, L. Marynowski, M. J. Fabiańska, M. Zatoń and B. R. Simoneit, Levoglucosan and other cellulose markers in pyrolysates of miocene lignites: Geochemical and environmental implications, *Environ. Sci. Technol.*, 2008, **42**(8), 2957–2963.
59 C. Mohr, J. A. Huffman, M. J. Cubison, A. C. Aiken, K. S. Docherty, j. R. Kimmel, I. M. Ulbrich, M. Hannigan and J. L. Jimenez, Characterization of primary organic aerosol emissions from meat cooking, trash burning, and motor vehicles with high-resolution aerosol mass spectrometry and comparison with ambient and chamber observations, *Environ. Sci. Technol.*, 2009, **43**(7), 2443–2449.
60 M. J. Cubison, A. M. Ortega, P. L. Hayes, D. K. Farmer, D. Day, M. J. Lechner, W. H. Brune, E. Apel, G. S. Diskin,

J. A. Fisher, H. E. Fuelberg, A. Hecobian, D. J. Knapp, T. Mikoviny, D. Riemer, G. W. Sachse, W. Sessions, R. J. Weber, A. J. Weinheimer, A. Wisthaler and J. L. Jimenez, Effects of aging on organic aerosol from open biomass burning smoke in aircraft and laboratory studies, *Atmos. Chem. Phys.*, 2011, **11**, 12049–12064.

61 H. Moosmüller and R. K. Chakrabarty, Technical note: simple analytical relationships between Ångström coefficients of aerosol extinction, scattering, absorption, and single scattering albedo, *Atmos. Chem. Phys.*, 2011, 11.

62 R. W. Bergstrom, P. Pilewskie, P. B. Russell, J. Redemann, T. C. Bond, P. K. Quinn and B. Sierau, Spectral absorption properties of atmospheric aerosols, *Atmos. Chem. Phys.*, 2007, **7**, 5937–5943.

63 T. W. Kirchstetter, T. Novakov and P. V. Hobbs, Evidence that the spectral dependence of light absorption by aerosols is affected by organic carbon, *J. Geophys. Res. Atmos.*, 2004, **109**, D21208.

64 Y. Chen and T. C. Bond, Light absorption by organic carbon from wood combustion, *Atmos. Chem. Phys.*, 2010, **10**(4), 1773–1787.

65 S. Segura, V. Estellés, G. Titos, H. Lyamani, M. P. Utrillas, P. Zotter, A. S. H. Prévôt, G. Močnik, G. L. Alados-Arboledas and J. A. Martínez-Lozano, Determination and analysis of in situ spectral aerosol optical properties by a multi- instrumental approach, *Atmos. Meas. Tech.*, 2014, **7**, 2373–2387.

66 D. A. Lack and J. M. Langridge, On the attribution of black and brown carbon light absorption using the Ångström exponent, *Atmos. Chem. Phys.*, 2013, **13**, 10535–10543.

67 J. C. Chow, L. W. A. Chen, X. Wang, M. C. Green and J. G. Watson, Improved estimation of PM2.5 brown carbon contributions to filter light attenuation, *Particuology*, 2021, **56**, 1–9.

68 T. C. Bond, S. J. Doherty, D. W. Fahey, P. M. Forster, T. Berntsen, B. J. DeAngelo, M. G. Flanner, S. Ghan, B. Kärcher, D. Koch, S. Kinne, Y. Kondo, P. K. Quinn, M. C. Sarofim, M. G. Schultz, M. Schulz, C. Venkataraman, H. Zhang, S. Zhang, N. Bellouin, S. K. Guttikunda, P. K. Hopke, M. Z. Jacobson, J. W. Kaiser, Z. Klimont, U. Lohmann, J. P. Schwarz, D. Shindell, T. Storelvmo, S. G. Warren and C. S. Zender, Bounding the role of black carbon in the climate system: a scientific assessment, *J. Geophys. Res. Atmos.*, 2013, **118**, 5380–5552.

69 G. Zhang, L. Peng, X. Lian, Q. Lin, X. Bi, D. Chen, M. Li, L. Li, X. Wang and G. Sheng, An Improved Absorption Ångström Exponent (AAE)-Based Method for Evaluating the Contribution of Light Absorption from Brown Carbon with a High-Time Resolution, *Aerosol Air Qual. Res.*, 2017, **19**(1), 15–24.

70 M. Gyawali, W. P. Arnott, K. Lewis and H. Moosmüller, In situ aerosol optics in Reno, NV, USA during and after the summer 2008 California wildfires and the influence of absorbing and non- absorbing organic coatings on spectral light absorption, *Atmos. Chem. Phys.*, 2009, **9**, 8007–8015.

71 D. A. Lack and C. D. Cappa, Impact of brown and clear carbon on light absorption enhancement, single scatter albedo and absorption wavelength dependence of black carbon, *Atmos. Chem. Phys.*, 2010, **10**, 4207–4220.

72 C. Liu, C. E. Chung, Y. Yin and M. Schnaiter, The absorption Ångström exponent of black carbon: from numerical aspects, *Atmos. Chem. Phys.*, 2018, **18**, 6259–6273.

73 D. Al Fischer and G. D. Smith, A portable, four-wavelength, single-cell photoacoustic spectrometer for ambient aerosol absorption, *Aerosol Sci. Technol.*, 2018, **52**(4), 393–406.

74 K. N. Liou, *An Introduction to Atmospheric Radiation*, Elsevier Science, 2nd edn, 2002.

75 J. H. Seinfeld and S. N. Pandis, *Atmospheric Chemistry and Physics: from Air Pollution to Climate Change*, John Wiley & Sons, Hoboken, NJ, 3rd edn, 2016, pp. 647–654.

76 M. Pitchford, W. Malm, B. Schichtel, N. Kumar, D. Lowenthal and J. Hand, Revised algorithm for estimating light extinction from IMPROVE particle speciation data, *J. Air Waste Manag. Assoc.*, 2007, **57**, 1326e1336.

77 M. Gysel, J. Crosier, D. O. Topping, J. D. Whitehead, K. N. Bower, M. J. Cubison, P. I. Williams, M. J. Flynn, G. B. McFiggans and H. Coe, Closure study between chemical composition and hygroscopic growth of aerosol particles during TORCH2, *Atmos. Chem. Phys.*, 2007, **7**, 6131–6144.

78 J. Hong, M. Äijälä, S. A. K. Häme, L. Hao, J. Duplissy, L. M. Heikkinen, W. Nie, J. Mikkilä, M. Kulmala, N. L. Prisle, A. Virtanen, M. Ehn, P. Paasonen, D. R. Worsnop, I. Riipinen, T. Petäjä and V. M. Kerminen, Estimates of the organic aerosol volatility in a boreal forest using two independent methods, *Atmos. Chem. Phys.*, 2017, **17**, 4387–4399.

79 V. A. Karydis, A. P. Tsimpidi, W. Lei, L. T. Molina and S. N. Pandis, Formation of semivolatile inorganic aerosols in the Mexico City Metropolitan Area during the MILAGRO campaign, *Atmos. Chem. Phys.*, 2011, **11**, 13305–13323.

80 G. Li, W. Lei, N. Bei and L. T. Molina, Contribution of garbage burning to chloride and $PM_{2.5}$ in Mexico City, *Atmos. Chem. Phys.*, 2012, **12**, 8751–8761.

81 M. Äijälä, K. R. Daellenbach, F. Canonaco, L. Heikkinen, H. Junninen, T. Petäjä, M. Kulmala, A. S. H. Prévôt and M. Ehn, Constructing a data-driven receptor model for organic and inorganic aerosol – a synthesis analysis of eight mass spectrometric data sets from a boreal forest site, *Atmos. Chem. Phys.*, 2019, **19**, 3645–3672.

82 A. Helin, J. V. Niemi, A. Virkkula, L. Pirjola, K. Teinilä, J. Backman, M. Aurela, S. Saarikoski, T. Rönkkö, E. Asmi and H. Timonen, Characteristics and source apportionment of black carbon in the Helsinki metropolitan area, Finland, *Atmos. Environ.*, 2018, **190**, 87–98, DOI: **10.1016/j.atmosenv.2018.07.022**.

83 P. Zotter, H. Herich, M. Gysel, I. El-Haddad, Y. Zhang, G. Močnik, C. Hüglin, U. Baltensperger, S. Szidat and A. S. H. Prévôt, Evaluation of the absorption Ångström

exponents for traffic and wood burning in the Aethalometer-based source apportionment using radiocarbon measurements of ambient aerosol, *Atmos. Chem. Phys.*, 2017, **17**, 4229–4249.

84 A. Burgos-Cuevas, D. K. Adams, J. L. García-Franco and A. Ruiz-Angulo, A Seasonal Climatology of the Mexico City Atmospheric Boundary Layer, *Boundary-Layer Meteorol.*, 2021, **180**(1), 131–154.

85 SEDEMA, Secretaría del Medio Ambiente de la Ciudad de México, *Inventario de emisiones de gases de efecto invernadero y carbón negro de la ZMVM 2008*, Mexico City, 2010.

86 SEDEMA, Secretaría del Medio Ambiente de la Ciudad de México, *Inventario de emisiones de gases de efecto invernadero y carbón negro de la Zona Metropolitana del Valle de México 2018*, Mexico City, 2021.

87 J. C. Cabada, A. Khlystov, A. E. Wittig, C. Pilinis and S. N. Pandis, Light scattering by fine particles during the Pittsburgh Air Quality Study: measurements and modeling, *J. Geophys. Res. Atmos.*, 2004, **109**, D16S03.

88 T. Moise, J. M. Flores and Y. Rudich, Optical properties of secondary organic aerosols and their changes by chemical processes, *Chem. Rev.*, 2015, **115**(10), 4400–4439.

89 L. I. Kleinman, A. J. Sedlacek III, K. Adachi, P. R. Buseck, S. Collier, M. K. Dubey, A. L. Hodshire, E. Lewis, T. B. Onasch, J. R. Pierce, J. Shilling, S. R. Springston, J. Wang, Q. Zhang, S. Zhou and R. J. Yokelson, Rapid evolution of aerosol particles and their optical properties downwind of wildfires in the western US, *Atmos. Chem. Phys.*, 2020, **20**, 13319–13341.

90 N. Barman, R. Roy, B. Saha, S. S. Kundu, A. Borgohain, B. K. De and A. Guha, Investigation of Seasonal Variation of Compensation Parameter and Absorption Ångström Exponent of Aerosol after Loading Correction over a Remote Station in North-East India, *Atmos. Environ.*, 2019, **212**, 106–115.

91 A. R. Kolhe, S. D. Ralegankar, P. D. Safai and G. R. Aher, Absorption properties of black carbon aerosols over environmentally distinct locations in south-western India: Temporal, spectral characterization and source apportionment, *J. Atmos. Sol. Terr. Phys.*, 2019, **189**, 1–17.

92 Y. Qiu, X. Wu, Y. Zhang, L. Xu, Y. Hong, J. Chen, X. Chen and J. Deng, Aerosol light absorption in a coastal city in Southeast China: temporal variations and implications for brown carbon, *J. Environ. Sci.*, 2019, **80**, 257–266.

93 B. L. Zhuang, T. J. Wang, J. Liu, Y. Ma, C. Q. Yin, S. Li, M. Xie, Y. Han, J. L. Zhu, X. Q. Yang and C. B. Fu, Absorption coefficient of urban aerosol in Nanjing, west Yangtze River Delta of China, *Atmos. Chem. Phys.*, 2015, **15**(23), 13633–13646.

94 K. M. Zhang, G. Allen, B. Yang, G. Chen, J. Gu, J. Schwab, D. Felton and O. Rattigan, Joint measurements of PM2. 5 and light-absorptive PM in woodsmoke-dominated ambient and plume environments, *Atmos. Chem. Phys.*, 2017, **17**, 11441–11452.

95 G. Carabali, J. Villanueva-Macias, L. A. Ladino, H. Alvarez-Ospina, G. B. Raga, G. Andraca-Ayala, J. Miranda, M. Grutter, M. M. Silva and D. Riveros-Rosas, Characterization of aerosol particles during a high pollution episode over Mexico City, *Sci. Rep.*, 2021, **11**, 22533.

96 C. Xie, W. Xu, J. Wang, Q. Wang, D. Liu, G. Tang, P. Chen, W. Du, J. Zhao, Y. Zhang, W. Zhou, T. Han, Q. Bian, J. Li, P. Fu, Z. Wang, X. Ge, J. Allan, H. Coe and Y. Sun, Vertical characterization of aerosol optical properties and brown carbon in winter in urban Beijing, China, *Atmos. Chem. Phys.*, 2019, **19**, 165–179.

97 Y. M. Qin, H. B. Tan, Y. J. Li, Z. J. Li, M. I. Schurman, L. Liu, C. Wu and C. K. Chan, Chemical characteristics of brown carbon in atmospheric particles at a suburban site near Guangzhou, China, *Atmos. Chem. Phys.*, 2018, **18**, 16409–16418.

98 C. S. Zhu, J. J. Cao, T. F. Hu, Z. X. Shen, X. X. Tie, H. Huang, Q. Y. Wang, R. J. Huang, Z. Z. Zhao, G. Močnik and A. D. Hansen, Spectral dependence of aerosol light absorption at an urban and a remote site over the Tibetan Plateau, *Sci. Total Environ.*, 2017, **590**, 14–21.

99 C. Li, Q. He, Z. Fang, S. S. Brown, A. Laskin, S. R. Cohen and Y. Rudich. Laboratory, Insights into the Diel Cycle of Optical and Chemical Transformations of Biomass Burning Brown Carbon Aerosols, *Environ. Sci. Technol.*, 2020, **54**(19), 11827–11837.

100 E. C. Browne, X. Zhang, J. P. Franklin, K. J. Ridley, T. W. Kirchstetter, K. R. Wilson, C. D. Cappa and J. H. Kroll, Effect of heterogeneous oxidative aging on light absorption by biomass burning organic aerosol, *Aerosol Sci. Technol.*, 2019, **53**(6), 663–674.

101 N. L. Ng, M. R. Canagaratna, Q. Zhang, J. L. Jimenez, J. Tian, I. M. Ulbrich, J. H. Kroll, K. S. Docherty, P. S. Chhabra, R. Bahreini, S. M. Murphy, J. H. Seinfeld, L. Hildebrandt, N. M. Donahue, P. F. DeCarlo, V. A. Lanz, A. S. H. Prévôt, E. Dinar, Y. Rudich and D. R. Worsnop, Organic aerosol components observed in Northern Hemispheric datasets from Aerosol Mass Spectrometry, *Atmos. Chem. Phys.*, 2010, **10**, 4625–4641.

102 N. L. Ng, M. R. Canagaratna, J. L. Jimenez, P. S. Chhabra, J. H. Seinfeld and D. R. Worsnop, Changes in organic aerosol composition with aging inferred from aerosol mass spectra, *Atmos. Chem. Phys.*, 2011, **11**, 6465–6474.

103 B. de Foy, J. R. Varela, L. T. Molina and M. J. Molina, Rapid ventilation of the Mexico City basin and regional fate of the urban plume, *Atmos. Chem. Phys.*, 2006, **6**, 2321–2335.

104 X. Fan, M. Li, T. Cao, C. Cheng, F. Li, Y. Xie, S. Wei, J. Song and P. Peng, Optical properties and oxidative potential of water- and alkaline-soluble brown carbon in smoke particles emitted from laboratory simulated biomass burning, *Atmos. Environ.*, 2018, **194**, 48–57.

105 G. Titos, A. Del Águila, A. Cazorla, H. Lyamani, J. A. Casquero-Vera, C. Colombi, E. Cuccia, V. Gianelle, G. Močnik, A. Alastuey, F. J. Olmo and L. Alados-Arboledas, Spatial and temporal variability of carbonaceous aerosols: assessing the impact of biomass burning in the urban environment, *Sci. Total Environ.*, 2017, **578**, 613–625.

106 G. R. McMeeking, E. Fortner, T. B. Onasch, J. W. Taylor, M. Flynn, H. Coe and S. M. Kreidenweis, Impacts of nonrefractory material on light absorption by aerosols emitted from biomass burning, *J. Geophys. Res. Atmos.*, 2014, **119**(12), 286.

107 M. Ealo, A. Alastuey, N. Pérez, A. Ripoll, X. Querol and M. Pandolfi, Impact of aerosol particle sources on optical properties in urban, regional and remote areas in the north-western Mediterranean, *Atmos. Chem. Phys.*, 2018, **18**, 1149–1169.

108 Y. Chen, X. Xie, Z. Shi, Y. Li, X. Gai, J. Wang, H. Li, Y. Wu, X. Zhao, M. Chen and X. Ge, Brown carbon in atmospheric fine particles in Yangzhou, China: light absorption properties and source apportionment, *Atmos. Res.*, 2020, **244**, 105028.